



rijksuniversiteit
 groningen



INTEGRATION PROJECT IEM

FACULTY OF SCIENCE AND ENGINEERING

Ocean Grazer: An analytical approach to design an umbilical cord & floater buoy system

Author

N. DANN RUIZ | S3388751

Supervisors

Prof. dr. A. VAKIS
Ir. T. M. KOUSEMAKER

June 12, 2020

Abstract

The depletion of natural resources and unceasing pollution of the planet have led to an urgent demand for alternative energy sources. The Ocean Grazer concept aims at contributing in covering such a gap. It consists of a floating offshore platform, that combines wave energy converters and wind turbines, and stores energy on-site. For operational purposes, a floater-umbilical system is required for both the prototype and full-scale platforms. Environmental loading from wind, waves, and currents, greatly determines the structural integrity of such a system. This study aims to determine an optimal outer sheath umbilical to withstand environmental loading, and design a floater buoy with the required buoyancy.

In this paper, an analytical approach is considered. Firstly, the static response of the prototype umbilical subject to environmental loading is studied. Environmental forces are obtained in a strictly analytical manner, and an optimisation problem is set up. It is found that the Factor of Safety (FOS), surge displacement and cable pretension are directly correlated. The study concluded the advantages of PVC as an outer sheath material. Secondly, the outer sheath armouring for the full-scale umbilical was designed. NEMOH, in combination with MATLAB, was implemented to obtain the wave excitation force. Environmental loading was then modelled on Solidworks Simulation and Solidworks Flow Simulation. The thickness of the armouring sheath was observed to be a key parameter to stabilise the floater-umbilical system against environmental loading, and an optimal thickness was presented.

List of Abbreviations

BEM	Boundary element method
DOF	Degree of freedom
FOS	Factor of safety
HDPE	High-density polyethylene
ID	Inner diameter
OD	Outer diameter
PE	Polyethylene
PUR	Polyurethane
PVC	Polyvinyl Chloride
UTS	Ultimate tensile strength
WEC	Wave energy converter

Contents

Introduction	1
I Research & Design Plan	2
1 Background Knowledge	3
1.1 Umbilical Cord	3
1.2 Floater Buoy	4
1.3 Umbilical Configurations	4
1.4 Equations of Motion	5
2 Problem Analysis	7
2.1 Problem Context	7
2.2 Stakeholder Analysis	8
2.3 System Description	9
2.4 Scope	9
2.5 Problem Statement	10
3 Research Goal	10
3.1 Goal Statement	10
4 Research Questions	10
5 Methodology	11
5.1 Matlab	11
5.2 NEMOH	12
5.3 Solidworks	12
II Prototype Umbilical	13
6 Umbilical Cord	14
6.1 Umbilical Components	14
6.2 Outer Sheath	15
6.3 Cable Length	15

7 Floater Buoy	16
7.1 Material Selection	16
7.2 Floater Buoy Design	17
8 Analytical Static Analysis	18
8.1 Analytical Calculations	18
8.1.1 Gravitational Force	19
8.1.2 Buoyancy Force	19
8.1.3 Drift Force	20
8.1.4 Wind Force	20
8.1.5 Current Force	21
8.2 Surge Displacement Analysis	21
8.2.1 Cable Pretension	25
III Full-scale Umbilical	27
9 Umbilical Cord	28
9.1 Umbilical Cross-section	28
9.2 Material Selection	28
9.3 Umbilical Design	29
10 Floater Buoy	29
11 Analytical Calculations	30
11.1 Buoyancy Force	30
11.2 Wind Force	31
11.3 Wave Excitation Force	31
11.4 Drag Force	33
11.5 Current Force	34
12 Simulation	34
12.1 Umbilical Design	34
12.2 Fixtures	35
12.3 Loads	35
12.3.1 Ocean Pressure	35
12.3.2 Current Force	35
12.3.3 Wave Excitation and Wind Force	36
13 Results	38
13.1 Analytical Static Analysis	38
13.2 Simulation Static Analysis	39
14 Discussion	41
14.1 Results Discussion	41
14.2 Limitations	41

14.3 Further Research	42
Conclusion	43
Bibliography	46
Appendices	47
A Material Properties	48
A.1 Polyvinyl Chloride (PVC)	48
A.2 High-density Polyethylene (HDPE)	49
B Technical Drawings	51
C Optimisation	53
D Static Surge Displacement Analysis	55
E Static Analytical Calculations	56
F Wave Characteristics	58
G Solidworks Fixtures and Meshing	59
H Loads Applied in Solidworks	60
I Surge Displacement Results	61
J Wave Excitation Results	63
K Solidworks Simulation Results	66

List of Figures

1	Ocean Grazer Concept	3
2	Cross-section of a high voltage power umbilical (sub, 2019)	4
3	Standard flexible umbilical configurations for floating offshore structures (Thies et al., 2012)	5
4	WEC-Sim coordinate system (wec, 2019)	6
5	Stakeholder matrix	8
6	System description	9
7	Diagram of research tools	11
8	Cross-section of prototype umbilical	15
9	Umbilical initial and equilibrium positions	16
10	Designed buoy	18
11	Free body diagram of floater buoy	18
12	Exploded view of designed buoy and simplified assembly	19
13	Drag coefficient for fixed circular cylinder and sphere for steady flow and smooth roughness (Schlichting and Gersten, 2000)	21
14	Static floater-cable system	22
15	Static floater-cable system at initial position	23
16	Static floater-cable system at equilibrium position	23
17	Elongation and surge displacement at equilibrium position	24
18	Deflection of straight beam	24
19	Variation of angular displacement and excitation force	26
20	Typical cross-sectional structure of subsea power umbilical cables	28
21	Preliminary umbilical cross-section	29
22	Discretisation and mesh of floater buoy	32
23	Surge excitation force plot for armouring thickness of 3 cm	33
24	Amplified view of the umbilical open air hose	34
25	Surface flow plot of current load	35
26	Surface flow plot of current load	36
27	Contour plot of current load	36
28	Resultant excitation force	37
29	Isometric view of loads and fixtures applied on the umbilical in Solidworks	37
30	Factor of safety for varying surge displacement	39
31	Surge displacement for $F_{pre} = 10420.820N$. Maximum displacement $\Delta x = 4m$	39
32	Plot of FOS against required umbilical buoyancy (kg)	40
33	Tensile strength (MPa) against density (kg/m^3)	49

34	Tensile strength (MPa) against price (EUR/kg)	49
35	Yield strength (elastic limit)(MPa) against density (kg/m^3)	50
36	Yield strength (elastic limit)(MPa) against price (EUR/kg)	50
37	Technical drawing of floating buoy	51
38	Exploded view and BOM of the assembly of the floater	52
39	Fixtures applied on the umbilical geometry in Solidworks	59
40	Mesh control applied on the umbilical geometry in Solidworks	59
41	Loads applied on the umbilical geometry in Solidworks	60
42	Surge displacements for $F_{pre} = 12505.816N$ (a) and $F_{pre} = 11978.400N$ (b).	61
43	Surge displacements for $F_{pre} = 11373.892N$ (a) and $F_{pre} = 10860.677N$ (b).	61
44	Surge displacements for $F_{pre} = 10420.820N$ (a) and $F_{pre} = 10040.649N$ (b).	62
45	Surge displacements for $F_{pre} = 9709.572N$ (a) and $F_{pre} = 9419.266N$ (b).	62
46	Surge displacement for $F_{pre} = 9163.120N$. Maximum displacement $\Delta x = 5$	62
47	Surge excitation for $t = 2.5cm$ (a) and $t = 2.75cm$ (b).	63
48	Surge excitation for $t = 3cm$ (a) and $t = 3.25cm$ (b).	63
49	Surge excitation for $t = 3.5cm$ (a) and $t = 3.75cm$ (b).	64
50	Surge excitation for $t = 4cm$ (a) and $t = 4.25cm$ (b).	64
51	Surge excitation for $t = 4.5cm$ (a) and $t = 4.75cm$ (b).	65
52	Surge excitation for $t = 5cm$ (a) and $t = 5.25cm$ (b).	65
53	Von Mises stress for a 3cm armouring thickness	66
54	FOS for a 3cm armouring thickness	66
55	Surge displacement for a 3cm armouring thickness	67

List of Tables

1	Overview of ongoing studies in the field of subsea umbilicals	8
2	Overview of deliverables, methods, and tools for each research question . . .	11
3	Description of prototype umbilical components	14
4	Minimum bending radius of umbilical components	15
5	Mechanical and physical properties of typical buoy	17
6	Buoyancy for half-submerged and full-submerged scenarios	20
7	Types of buoys	30
8	Inputs to axiMesh.m function	32
9	Results	38
10	Results for varying armouring layer thickness	40
11	PVC (Semi-rigid, molding and extrusion) properties (Cambridge, 2014) . . .	48

Listings

1	Inputs for mesh generation	31
2	Inputs for mesh generation	33
3	File of inputs and minimization options (main.m)	53
4	Objective function (objective.m)	54
5	Constraints function for the solver (nlcon.m)	54
6	Static surge displacement	55
7	Buoy dimensions script	56
8	Wavenumber script	58
9	Wave velocities script	58

Introduction

Greenhouse gasses released during the combustion of fossil fuels are accountable for 76% of global greenhouse emissions (fos, 2016). Scarcity of natural resources, together with the increasing temperature and pollution of the planet, have led to an urgent demand for alternative energy sources. The renewable energy sector is undergoing growth and development as a sustainable energy source to tackle these issues (Khan and Ulucak, 2020). Over the years, the industry has undergone vast technological advances in the fields of solar, wind and wave energy, making the technology mature and not as costly, therefore requiring fewer government subsidies (gov, 2018). To be competitive in the sector, a feasible model is required. Ocean Grazer is a Dutch company founded in 2014 with the objective of generating renewable energy and supplying it on demand. It produces renewable offshore energy by combining wave energy converters with wind turbines, and stores it on-site. Ocean Grazer has developed the Ocean Battery, which is located on the ocean bed. The design of an umbilical cord and floater buoy, that connect the Ocean Battery to the sea surface, is required for operational purposes. The research presented here focuses on the development of such a system, by analysing the existing scaled-down prototype and later designing the full-scale system through analytical methods. In particular, the focus relies on the design of the floater buoys for each system, and on the study of the outer sheath of the umbilicals subjected to environmental loading. A floater for the existing prototype umbilical will first be developed, and analytical calculations on environmental loading will enable this paper to perform a surge displacement analysis. Afterwards, a second floater buoy will be developed for the full-scale version, and a static analysis on the forces acting on the cable will be executed. The outputs of this study will allow this paper to draw conclusions on the optimal outer sheath armouring.

Part I

Research & Design Plan

1 Background Knowledge

The Ocean Grazer is an offshore renewable energy harvesting concept, currently being developed and researched by the University of Groningen. Ocean Grazer intends to use the full potential of ocean energy by combining technologies into one hybrid device. Figure 1 gives an overview of the current floating platform concept. It combines wave energy converter technology with on-site energy storage and wind turbines to generate and store renewable energy offshore. Ocean Grazer will be launching a scaled-down prototype of the platform in the summer of 2020. Further on, it aims to deploy a floating platform in the ocean by 2022.

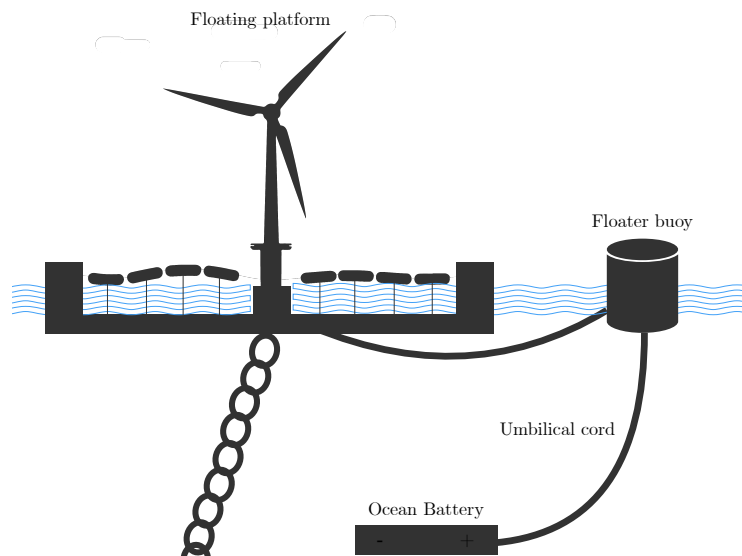


Figure 1: Ocean Grazer Concept

The umbilical cord and floater buoy are the focus of this project. This is a sub-sea system of power lines, transmission cables and air hoses to transport electricity and operate the Ocean Battery, with a floating connection point at the surface. The following sections give an overview of these elements.

1.1 Umbilical Cord

A subsea umbilical consists of a combination of electrical cables, fiber-optic cables, steel tubes, and thermoplastic hoses, to execute a specific function (Bai and Bai, 2012). Within the offshore industry, these functions range from providing hydraulic pressure for activating valves, to chemical or gas injection. Figure 2 depicts the typical cross-section of a high power umbilical cable. Electricity transmission via subsea power cables is a well-established technology that has been in use for more than a century (Worzyk, 2009).

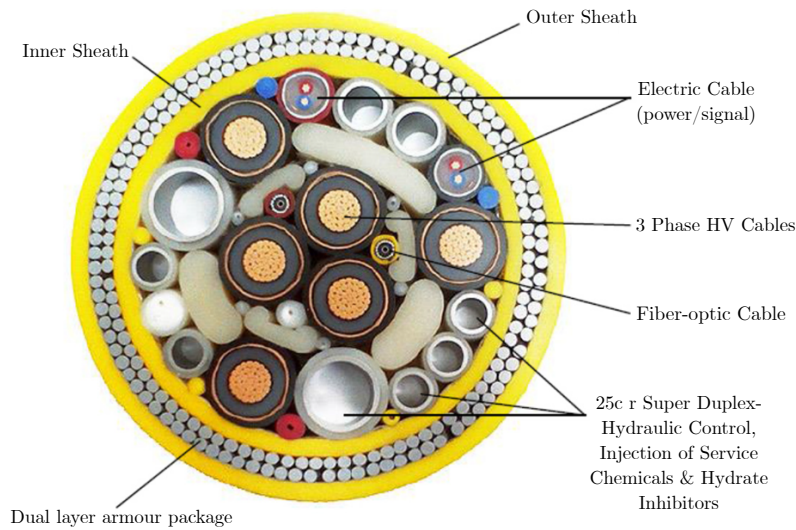


Figure 2: Cross-section of a high voltage power umbilical (sub, 2019)

For Ocean Grazer, the purpose of the umbilical system differs between the scaled-down and final energy plants. For the scaled-down prototype, the umbilical is designed for electricity transmission, communication and pressure equalising purposes. The cable will allow the Ocean Battery to charge and discharge when required, together with locking the supporting reservoir of the battery to the ocean bed by equalising pressures through an air hose. In the full-scale version, the umbilical will solely serve the purpose of pressure equalising.

1.2 Floater Buoy

Ocean Grazer intends to create an advanced buoy for its floating platform. This buoy will be capable of determining whether to store electricity in the Ocean Battery, or to supply it to the grid. This will create a smart grid, in which storage or sale of electricity is determined in relation to the generated and demanded electricity. Within the floater buoy, a device will be contained that acts as a control system. As this project is at an early research stage, the floater buoy must first be developed. This research will focus merely on the design of a floater buoy for the umbilical cable, and not taking into account its actual role within the electricity grid.

1.3 Umbilical Configurations

The umbilical system can be designed into different ‘shapes’, or umbilical configurations. The factors that determine an optimal umbilical configuration are primarily the depth of operation and loading regimes (Clausen and D’Souza, 2001). Figure 3 depicts the three standardised configurations for flexible umbilicals (Thies et al., 2012). To achieve different umbilical configurations, underwater floaters are attached to the umbilical line. Typically, lazy wave and free-hanging catenary configurations are employed for larger depths. Their stability against environmental loading has been modelled by Thies et al. (2012) and Martinelli et al. (2010) at depths of 57 and 250 meters respectively. It was found that the lazy wave reduces maximum tension forces, avoids compression, and has fewer fatigue cycles.

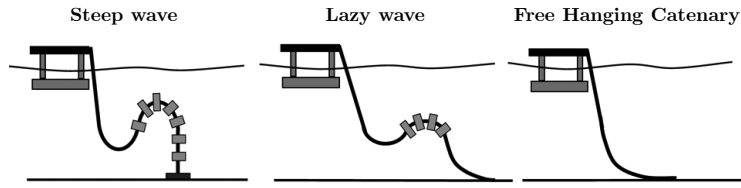


Figure 3: Standard flexible umbilical configurations for floating offshore structures (Thies et al., 2012)

This thesis will focus on the study of a free-hanging catenary cable. On the one hand, the prototype umbilical has been developed in a catenary configuration, due to its deployment at the testing harbour. Under steady water conditions, reduction of environmental forces is not required. On the other hand, the analytical methods utilised in this paper, which will be further discussed in Section 5, will only deliver reliable results for a catenary configuration. Despite the aforementioned studies proving the lazy wave to be more favourable, the catenary is still widely used in the offshore industry. Moreover, adopting a lazy wave shape incurs an additional capital cost factor, due to its buoyancy elements and a longer overall length (Rentschler et al., 2020).

1.4 Equations of Motion

It is imperative to describe the equations governing the motion of the object at study. In this case, the system can be seen as a floating body moored to the sea bed. The coordinate system used is depicted in Figure 4. The incident waves are considered to come in the x -direction (surge) direction. In this study, the incident waves are taken to be regular. These are defined as planar sinusoidal waves, where the incident wave is defined as:

$$\eta(x, y, t) : \frac{H}{2} \cos (wt - k(x \cos \theta + y \sin \theta) + \phi) \quad (1)$$

where H is the wave height, w is the wave frequency ($w = \frac{2\pi}{T}$), k is the wavenumber ($\frac{2\pi}{\lambda}$), θ is the wave direction, and ϕ is the wave phase. The coordinate system presented is a 6 degree of freedom (DOF) system, depicted in Figure 4. In this system, the translatory displacements (forces) in x -, y - and z - directions are defined as surge, sway and heave; and angular displacement in the same order of axes (moments) are defined as roll, pitch and yaw. However, due to the symmetry of the body shape and the mooring stiffness, the degrees of freedom can be limited to the following three: Surge, heave and pitch. Due to the limitations of the implementation of NEMOH, the calculations are required to be represented in 6 DOFs.

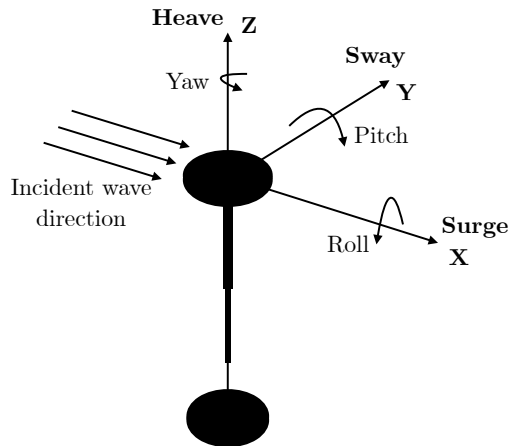


Figure 4: WEC-Sim coordinate system (wec, 2019)

Wave forcing components are typically modelled using linear coefficients obtained from a frequency-domain potential flow Boundary Element Method (BEM). The equations of motion will thus be formulated in the frequency domain. In accordance with Wei et al. (2017), the equation of motion in one DOF for a floating buoy about its center of gravity is given as:

$$m\ddot{z} = F_{ex} + F_{rad} + F_{hs} \quad (2)$$

where F_{ex} is the vector of excitation forces and moments. F_{rad} is the force and torque vector resulting from wave radiation. It can be described through an added mass term and a hydrodynamic damping term as follows:

$$F_{rad} = -m_a(w)\ddot{z}(w) - c(w)\dot{z} \quad (3)$$

where $m_a(w)$ is the added mass coefficients matrix, and $c(w)$ is the damping coefficients matrix. Both of these hydrodynamic coefficient matrices are provided by NEMOH. Furthermore, F_{hs} is the restoring force vector, which arises when the floater is perturbed away from its equilibrium position. It can be described as (Wei et al., 2017):

$$F_{hs} = -k_{hs}z \quad (4)$$

where k_{hs} corresponds to the hydrostatic stiffness matrix that specifies the variation of the net weight and buoyancy load with respect to the changes in position from equilibrium (Faltinsen, 1993). This matrix will also be retrieved from NEMOH. Combining Equation 3 and Equation 4 into Equation 2, and rearranging in terms of F_{ex} yields:

$$(m + m_a(w))\ddot{z} + c\dot{z} + k_{hs}z = F_{ex} \quad (5)$$

The vector for displacement, velocity and acceleration is defined as:

$$z = \begin{bmatrix} z \\ \dot{z} \\ \ddot{z} \end{bmatrix} \quad (6)$$

This vector can be expressed in either frequency or time domain. A frequency domain representation will be utilised, as all the parameters are either constants or frequency dependent. The vector is then defined as:

$$z = \begin{bmatrix} z(t) \\ \dot{z}(t) \\ \ddot{z}(t) \end{bmatrix} = \begin{bmatrix} \hat{z}(w)e^{iwt} \\ iw\hat{z}(w)e^{iwt} \\ -w^2\hat{z}(w)e^{iwt} \end{bmatrix} \quad (7)$$

and

$$F_{ex}(t) = \hat{F}_{ex}(w)e^{iwt} \quad (8)$$

Plugging in Equation 7 and Equation 8 into Equation 5 yields:

$$[-w^2(m + m_a) + iwc(w) + k_{hs}]\hat{z} = \hat{F}_{ex}(w) \quad (9)$$

This equation of motion needs to be solved for every DOF of the floater. For 6 DOFs Equation 9 is described as follows:

$$[-w^2(M + M_a) + iwX(w) + K_{hs}]\hat{Z} = \hat{F}_{ex}(w) \quad (10)$$

where \hat{z} had been defined as the displacement in the z-direction of the body, and \hat{Z} is a 1x6 vector representing the displacement in surge, sway, heave, roll, pitch and yaw direction. Furthermore, M and $M_a \in \mathbb{R}^{6 \times 6}$ are the diagonal matrices for mass and the moments of inertia of the buoy. Similarly, $C \in \mathbb{R}^{6 \times 6}$ is the matrix of damping coefficients, and $K_{hs} \in \mathbb{R}^{6 \times 6}$ is the matrix of stiffness coefficients. Finally, \hat{F}_{exc} is the 1x6 vector of excitation forces in 6 DOFs.

2 Problem Analysis

2.1 Problem Context

The rapid emergence of the floating offshore energy sector requires the development of new technologies, such as the floating platform currently being developed by Ocean Grazer. The problem owner, the Chief Technology Officer of Ocean Grazer (Subsection 2.2), requires the design of an umbilical cord and floating buoy system. Many factors play a role in the design of such a system, and numerous challenges need to be tackled to ensure a stable system. Research and literature in the field point towards various relevant factors that will affect the structural integrity and service lifetime. The existing body of knowledge is summarised in Table 1.

Nr.	Authors	Factors	Description
1	Research study by Yang et al. (2018a)	Environmental loads	Motions of the Wave Energy Converter (WEC), motion of the platform, wave loads, and currents.
2	Simulation studies by Chang and Chen (2019) and Thies et al. (2012)	Cable loading	Mechanical loading, fatigue, tension, torsion and compression loads acting of the floating cable

Nr.	Authors	Factors	Description
3	Research study by Keresten et al. (2019)	Structure and armour of umbilical	Study of the optimal stiffness of the cable
4	Research study by Yang et al. (2018b)	Cable components	Optimal cross sectional design of its components
5	Research study by Patel (2008)	Cable installation	Failure by incorrect installation, electrical flaws, manufacturing and operational practices

Table 1: Overview of ongoing studies in the field of subsea umbilicals

When focusing on the outer sheath of the umbilical cable, its armouring is a vital element. Factors such as its mechanical strength, stiffness, and flexibility will determine the behaviour of the floating cord, and thus its stability (Martinelli et al., 2010). The cable is continuously subjected to bending and twisting forces, caused by the tidal current and floater behaviour, therefore making it susceptible to mechanical failure. Indeed, the outer sheath material will determine mechanical failure modes. These range from tensile failure, bending failure, excessive twisting, compression and fatigue to abrasive friction on the seabed (Rentschler et al., 2020).

2.2 Stakeholder Analysis

A stakeholder analysis was performed as a tool to understand who the problem is relevant to, and what their role and power over the research is. Three stakeholders were determined, and have been placed in a Mendelow’s diagram, illustrated in Figure 5.

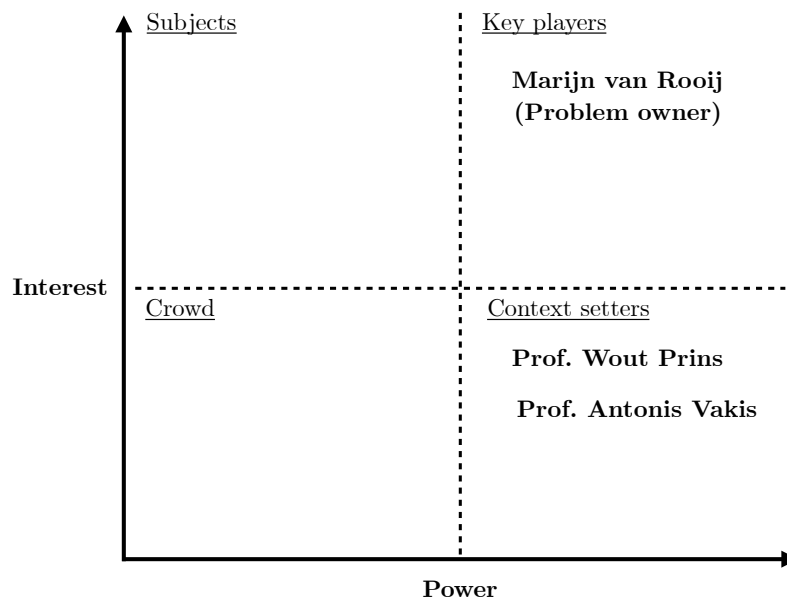


Figure 5: Stakeholder matrix

- Marijn van Rooij: Marijn is the Chief Technology Officer (CTO) of Ocean Grazer, and is considered the problem owner. He has high interest and power in the project. As the problem owner, it is his stake in the company to tackle this issue, and thus has high interest

in the outcome of the research. Moreover, he has steering power, and can decide what is the scope of the research.

- Professor Antonis Vakis: Professor Vakis represents the University of Groningen, and is the supervisor of the project. Moreover, he serves as a scientific advisor for Ocean Grazer, and has been described as a context setter. He is particularly concerned about the methodology and validity of the findings of this research, but not as concerned about how they aligned with the company objectives.
- Wout Prins: Mr Prins is the co-founder and a large shareholder of the Ocean Grazer Company. He is also considered a context setter, as his only concern is that the outcome is in line with the company objectives.

In conclusion, close coordination with Marijn is required, to ensure an understanding of his needs, and to make sure the deliverable meets his requirements. Moreover, there is no conflict between stakeholders, and Antonis and Wout will serve as advisors.

2.3 System Description

The system will be delineated to consist of a floater buoy, moored to the Ocean Battery through the umbilical line. The type of Ocean Battery connection will be neglected in this study, and assumed to be a simple fixture of the cross-sectional surface of the umbilical to the sea bed. Figure 6 shows the described system at study, with the aforementioned catenary configuration.

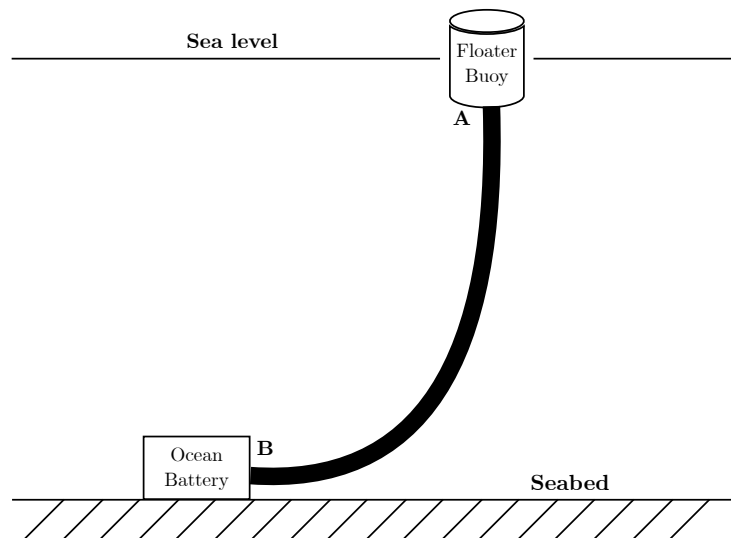


Figure 6: System description

2.4 Scope

For the scheduled duration of this research, and in order to deliver detailed reliable results, the scope of the project must be narrowed down. The scope will be delineated to the static study of the influence of environmental loading from waves, wind, and currents on the system. Firstly, a floater buoy will be designed for the existing prototype umbilical. An analytical static surge displacement will then be performed to study the loading on the outer sheath material, and determine its validity. Secondly, the full-scale umbilical will be designed, together with a floater buoy that withstands the umbilical weight. A static analysis of environmental loading will again be performed, in order to determine and optimal outer sheath umbilical design.

2.5 Problem Statement

Based on the problem context and wishes of the problem owner, the following problem statement can be derived.

“For Ocean Grazer to develop a floating energy platform by 2022, the design of an umbilical cord and floater buoy is required. At an early research stage, Ocean Grazer requires the development of a floater buoy for the launch of a scaled-down platform in the Summer of 2020, and the preliminary design of a floater buoy and outer sheath material for the umbilical for the launch of the full-scale platform in 2022. Numerous factors play a role in the deployment of a stable and durable umbilical system. The environmental forces acting on the system, and the material and structural properties of its elements are critical design aspects, and need to be addressed. Hydrostatic loading on the floater buoy from waves, wind, and currents will affect the behaviour of the buoy, and will, in turn, determine the loading on the umbilical cord. Moreover, the large pressures at the ocean bed will challenge the integrity of the umbilical. A static analysis on these forces is required, coupled with a mathematical simulation method, to determine the loading on the system.”

3 Research Goal

3.1 Goal Statement

From the problem statement and the request from Ocean Grazer to create a prototype of a umbilical and advanced buoy system, the following research goal can be derived.

“The goal of this research is to deliver Ocean Grazer with a design of the floater buoys for both the full-scale and prototype floating platforms, and to determine an optimal outer sheath armouring for the umbilical in the full-scale floating platform, by first determining the external environmental forces acting on the floater buoy, and then studying the umbilical response in terms of stress, to determine and optimal outer sheath layer. For the intended duration of a Bachelor thesis project, the two deliverables: the floater for the scaled-down model and the floater and outer sheath umbilical for the full-scale umbilical; will be developed in a period of 12 weeks.”

4 Research Questions

1. CQ1: What is the static response of the prototype umbilical cord to hydrostatic loads in terms of cable force and displacement?
 - I What is the desired buoy geometry?
 - II What is the environmental loading from waves and currents acting on the floater buoy?
 - III What is the allowable buoy displacement?
 - IV What is the effect of cable pretension on the allowable surge displacement?
2. CQ2: What is a feasible design for the outer sheath layer of the umbilical for operation in all weather and ocean conditions?
 - I What is the relation between varying the thickness of the armouring layer of material and the buoy geometry?

- II What is the effect of varying the thickness of the armouring layer of material in terms of wind and current loading?
- III What is the surge excitation force on the buoy from incident waves?
- IV What is an accurate way of simulating the static loads on the umbilical?

5 Methodology

In order to answer the research questions, a compatible research strategy and a set of tools have to be selected. Table 2 gives an overview of the deliverables, methods, and tools which will be utilised to obtain answers to the research questions.

Question	Deliverable	Strategy	Tool
1.1	Mathematical model to simulate static response to external ocean forces	Desk research	Solidworks MATLAB
1.2		Desk research Mathematical experimentation	
1.3		Desk research	
1.4		Mathematical experimentation	
2.1	Optimal thickness of umbilical armouring layer	Mathematical experimentation	NEMOH Solidworks MATLAB
2.2		Mathematical experimentation	
2.3		Programming	
2.4		Programming	

Table 2: Overview of deliverables, methods, and tools for each research question

A schematic overview of the tools that will be utilised throughout this project is depicted in Figure 7. These tools will be further discussed.

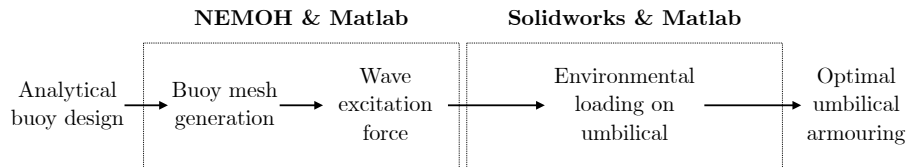


Figure 7: Diagram of research tools

5.1 Matlab

MATLAB is a numerical computing environment that enables solving engineering problems through computational mathematics. MATLAB will be the pillar of this thesis, as it will be used both as a wrapper for the fluid-body simulation program NEMOH, and for writing scripts for analytical calculations.

5.2 NEMOH

NEMOH is an open source code used for the computation of first-order wave loads on offshore structures. It is a boundary element method (BEM) model based on linear potential flow theory, which solves the linear boundary value problems (BVPs). The main outputs are the hydrostatic stiffness matrix, and the first order hydrodynamic coefficients for added mass, radiation damping and excitation force. It will be utilised to mesh the floater buoy geometry, determine the wave excitation force on the structure, and ultimately its stability.

5.3 Solidworks

Solidworks is a computer-aided design program that enables to run engineering simulations on solid geometries and assemblies. The Solidworks Simulation add-in will enable to apply the environmental loads on the umbilical geometry, and obtain static results in terms of stress and displacement of the structure. Furthermore, the Solidworks Flow Simulation add-in will be utilised to simulate the effect of the ocean current on the umbilical geometry.

Part II

Prototype Umbilical

6 Umbilical Cord

The prototype umbilical serves the purposes of electricity transmission, communication and pressure equalising between the surface and Ocean Battery. This prototype will be operating at the testing harbour. The operating depth of the umbilical is 3-5 meters, due to tidal variation.

6.1 Umbilical Components

The umbilical components, their specifications, and functions are described in Table 3. The cross-sectional layout of the umbilical is depicted in Figure 8.

Component	Specifications	Function
Outer sheath	PVC Dragflex Ultraflex suction hose	Protect umbilical components
Air-ventilation hose	PVC Dragflex Ultraflex suction hose \varnothing 35 x 25 mm	Equalise pressure between the Ocean Battery reservoir and ocean surface
Data cable 1	CAT5E, 6, 6a or 7, Shielded \varnothing 6.2 mm, 8 cores	Information transmission between Ocean Battery and ocean surface
Data cable 2	CAT5E, 6, 6a or 7, Shielded \varnothing 6.2 mm, 8 cores	Back-up data cable in case of failure of Data cable 1
Pneumatic air-hose 1	Nylon, max 8 bar \varnothing 8 x 5.5 mm	Pump air to Ocean Battery to operate its valves
Pneumatic air-hose 2	Nylon, max 8 bar \varnothing 8 x 5.5 mm	Pump air to Ocean Battery in case of emergency or need of repair. The battery will float up to the surface.
Powersupply cable	230V, 16A \varnothing 8.2, 3 x 1.5 mm ²	Supply electricity from Ocean Battery to the surface.
Turbine power cable	230V, 16A \varnothing 8.2, 3 x 1.5 mm ²	Transport generated electricity to the Ocean Battery
Water hose	Nylon, max 8 bar \varnothing 10, 3 x 7.5 mm	To fill up Ocean Battery reservoir.

Table 3: Description of prototype umbilical components

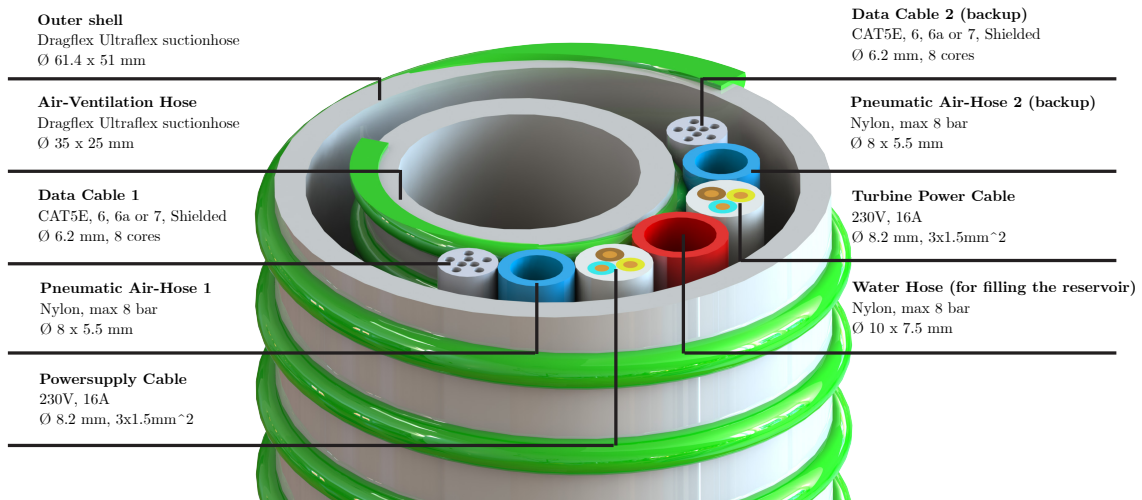


Figure 8: Cross-section of prototype umbilical

6.2 Outer Sheath

For this preliminary prototype umbilical, the PVC Dragflex UltraFlex suctionhose, manufactured by PVC Voordeel, was deemed to meet the operational requirements by the CTO of Ocean Grazer. The material and mechanical properties of polyvinyl chloride (PVC) are gathered in Appendix A.1. Overall, it is an advantageous material due to its mechanical strength and toughness, great resistance to water, being light weight, durable, easy to install and cost-effective. To protect the umbilical components, the outer sheath should be stiffer than the elements contained. The flexibility of each component was found, and is gathered in Table 4 in terms of minimum bending radius. Indeed, the PVC outer sheath is the stiffest component. The validity of flexible PVC as an outer sheath material will be examined analytically in Section 8.

Component	Specifications	Min. bending radius	Max. operating pressure	Reference
Data cable	CAT6A Hard nylon	25 mm	n.a	cat (2019)
Water hose	OD 10 mm ID 7.5 mm	60 mm	24 bar	wat (2019)
Air hose	OD 8 mm ID 5.5 mm 230V 16A	22 mm	19 bar	wat (2019)
Power supply cable	OD 8.2 mm $3 \times 1.5m^2$	58 mm	n.a	wat (2019)
Air pressuriser	OD 35 mm ID 25 mm	280 mm	n.a	PIPA (2016)
Outer sheath	OD 61.4 mm ID 51 mm	614 mm	n.a	PIPA (2016)

Table 4: Minimum bending radius of umbilical components

6.3 Cable Length

The various forces considered to be acting on the floater buoy, explained in Section 8, result in a displacement of Δx . These forces are assumed to act on the floater in the surge direction, in accordance with Figure 9, and result in the movement of the floater to an equilibrium position.

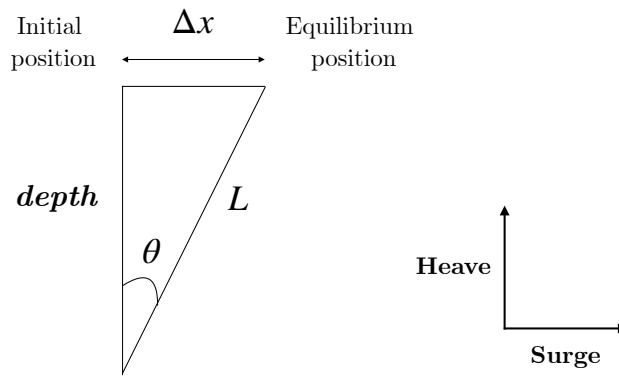


Figure 9: Umbilical initial and equilibrium positions

A large displacement will interfere with the operation of the platform, and is not desired. The cable length L should thus be designed to minimise such a displacement. This can be achieved by setting the cable length equal to the largest depth considered, that is, $L = 5$ meters. This will result in a maximum displacement of:

$$\Delta x = \sqrt{L^2 - \text{depth}^2} = \sqrt{5m^2 - 3m^2} = 4m \quad (11)$$

for the limiting case scenario of a depth of 3 meters.

7 Floater Buoy

To withstand the weight of the umbilical, an appropriate floater must be selected. This section will discuss the optimal material and design for the floater buoy.

7.1 Material Selection

The desirable material characteristics when designing a floating structure or buoy are: nontoxic, resistant to saltwater and alkalis acids, UV resistant, recyclable, and to be able to withstand temperatures from -60°C to 80°C for an extended period of time underwater without retrograde in its mechanical properties (Granqvist, 2003). The floater solutions for these conditions are plastic and stainless-steel elements (Sahu et al., 2019). Since metals are very costly, and less resistive to various chemicals present in water bodies, plastic floats become more favourable (Sahu et al., 2019). Thermoplastics will thus be the focus of the material selection, due to their light weight and good strength and resistive properties.

The use of polyolefins has increased significantly in recent decades, and are very attractive due to their low cost, good mechanical properties, light weight, durability and versatility with respect to other materials (Ammalaa et al., 2010). Most of the buoys commercially available have a high-density polyethylene (HDPE) shell and a polyurethane (PUR) core, which is usually in the form of foam (Beirão and Malça, 2014). Moreover, the use of standard polyethylene (PE) is also customary in the industry. The relevant mechanical, physical general properties of these are gathered in Table 5.

Material	HDPE	PE	PUR
Young's Modulus	1.08 GPa	1.2 GPa	1.69 GPa
Yield Strength	28.6 MPa	19 MPa	46.9 MPa
Density	958.5 kg/m ³	1080 kg/m ³	1180 kg/m ³
Price	1.39 EUR/kg	3.11 EUR/kg	4.61 EUR/kg
Durability Water (salt)	Excellent	Acceptable	Excellent
Durability UV radiation	Fair	Fair	Fair
Durability strong alkalis	Excellent	Excellent	Limited use
Recyclability	Yes	Yes	No

Table 5: Mechanical and physical properties of typical buoy

The density of the material is an imperative design factor, as it will determine the buoyancy of the floater. The lower the density, the more buoyant the floater will be. It can be observed that HDPE has the lowest density, making it more buoyant, with a lower density than ocean water, which is defined to be 1027 kg/m^3 for the North Sea. Another imperative factor is the resistance to environmental phenomena, such as visible light and ultra-violet (UV) radiation. It is known that polymeric and other materials can lose mechanical properties from ageing environments (Platzer, 1986) (Feldman, 1984). For this reason, durability against UV light is defined to be 'fair'.

HDPE has governed a dominating position because of the many excellent properties, cost and ease of fabrication and modifications to enhance its mechanical properties (Sahu, 2017). Due to its lower density than water, it has been widely used as a supporting platform for the arrangement of solar panels over the surface of water bodies (Sahu et al., 2016). Furthermore, a lower Young's Modulus results in a more flexible material, which is optimal for a buoy. Moreover, an experimental study by Ammalaa et al. (2010) on the weathering conditions of HDPE found that the mechanical properties of HDPE after accelerated UV exposure were not much affected, and it is safe to bear the load of solar panels and other accessories mounted on it. Additionally, PE and HDPE are thermoplastic resins, making them recyclable, whereas PUR is a thermoset resin, making it unsuitable for recycling (Brent, 2019). For these reasons, the material chosen is high-density polyethylene (HDPE), as its properties will be advantageous in mooring applications. Refer to Appendix A.2 for further plots of the yield and tensile strength against the price and density of the material. These graphs are plotted for all polymers, and the position of HDPE is labelled. The plots evidence the profitable properties of the material with respect to other polymers.

7.2 Floater Buoy Design

An optimal design, which is typically used for these applications, consists of two semicircular 'shells' that clamp around the upper-end of the umbilical. This particular design, is optimal for distributing loading at the connection point with the umbilical. With a larger contact surface, axial and torsional loads are better distributed. Furthermore, the chamfered edges reduce drag motion caused by environmental forces. Figure 10 illustrates the designed buoy. The two HDPE 'shells'

are held together by means of two sets of nuts and bolts with washers in between. The detailed technical drawings of the floater buoy, and the exploded assembly are depicted in Figure 37.

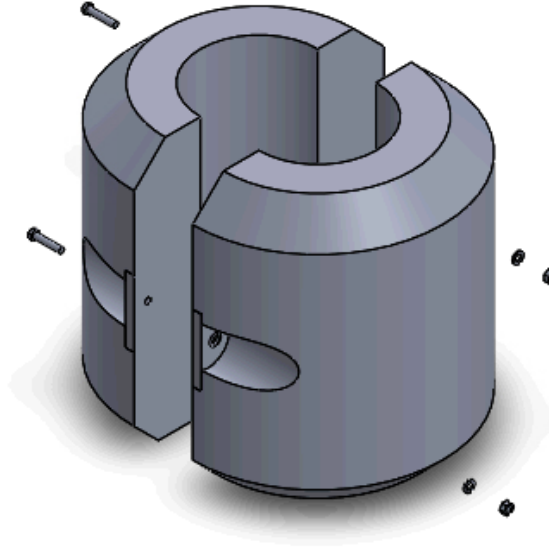


Figure 10: Designed buoy

8 Analytical Static Analysis

8.1 Analytical Calculations

In this section, the forces acting on the floater buoy will be calculated analytically. These forces are depicted in the free body diagram in Figure 11. With regards to the submersion of the buoy, an assumption will be performed: it is assumed that the buoy is half-submerged in the ocean. The forces acting on the body will be further discussed in the following sections.

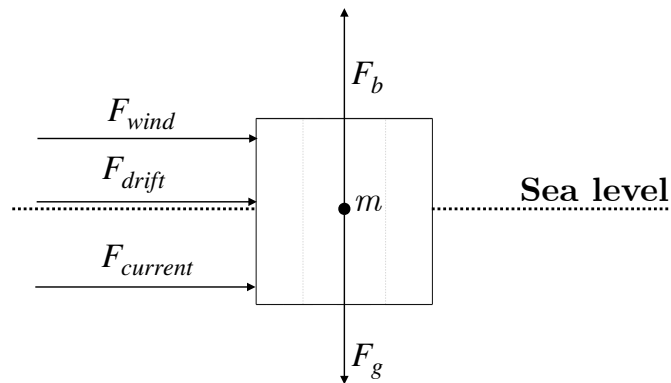


Figure 11: Free body diagram of floater buoy

Furthermore, for simplicity of calculation, the geometry of the floater will be assumed to be cylindrical, as shown in Figure 12(b). The simplification of the chamfered edges will influence the results insignificantly.

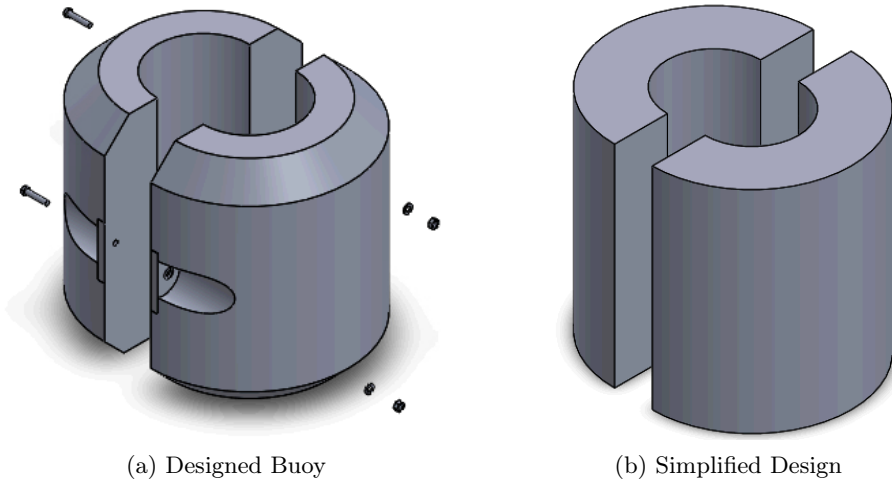


Figure 12: Exploded view of designed buoy and simplified assembly

8.1.1 Gravitational Force

The gravitational force created by a certain mass m can be computed as

$$F_g = mg \quad (12)$$

Where g is the gravitational acceleration with a known value of $9.81m/s^2$. Considering that the average value of a buoy of these dimensions is $20kg$ (Telleborg, 2020), the respective gravitational force is

$$F_g = 20kg \times 9.81m/s^2 = 196.2N \quad (13)$$

8.1.2 Buoyancy Force

The buoyancy force is caused by the tendency of a fluid to occupy the space taken by the object in the medium. By Archimedes' principle, the buoyant force on an object is equal to the weight of the fluid displaced by the object, given by:

$$F_b = \rho_w V_o g \quad (14)$$

where ρ_w is the density of the liquid and V is the volume of the submerged object. The density of seawater will be considered, and the value of $1027kg/m^3$ will be taken. The volume V_o , is the volume of the buoy that is submerged, that is, half of the total volume of a cylinder $V_o = \frac{1}{2}V_{cylinder}$. Moreover, it is imperative to validate the designed buoy, by calculating its maximum buoyancy. Maximum buoyancy of the floater occurs when it is fully submerged, therefore having a volume of $V_{max} = V_{cylinder}$. The obtained buoyancy force values are gathered in Table 6.

	Half-submerged	Full-submerged
Volume submerged (m^3)	0.059	0.188
Buoyancy force (N)	594.42	1188.83

Table 6: Buoyancy for half-submerged and full-submerged scenarios

The resulting force being exerted by the buoy, based on Figure 11, is the following summation in the y-direction:

$$\sum F_y = F_{bmax} - F_g = 1188.83N - 196.2N = 992.63N \quad (15)$$

The maximum load that the floater can withstand is:

$$m = \frac{\sum F_y}{g} = 101.19kg \quad (16)$$

Under the formulated set of assumptions, the buoy can withstand a load of 101.19 kilograms. Furthermore, the umbilical has a buoyancy force of its own, greatly increased by the air-ventilation hose. For this reason, and due to its low weight for its small length for $L = 5$ meters, the buoy can be concluded to be sufficient.

8.1.3 Drift Force

In this analysis, it is assumed that the wave is completely absorbed by the buoy. As described by Fonseca et al. (2008), the simplified formula for the wave drift force is:

$$F_d = \frac{1}{4}\rho_w g H^2 \quad (17)$$

where H is the wave amplitude in meters.

8.1.4 Wind Force

The mean wind force is calculated based by means of the drag force equation (A. Nesegard and Bitner-Gregersen, 2010). The formula for mean wind force is:

$$F_w = \frac{1}{2}\rho_a C A U_w^2 \quad (18)$$

Where ρ_a is the density of air, C is the shape coefficient, A is the area exposed to wind and U_w the mean wind velocity. For an average air temperature of the North Sea of $10.5^\circ C$ (avg, 2012), the air density ρ_a is $1.244kg/m^3$ (air, 2020). The average wind speed U for the North Sea coast is taken as $7.8m/s$ (Coelingh et al., 1996). The shape coefficient, or drag coefficient C for a cylinder is a factor of the Reynolds number Re , and the roughness of the cylindrical body (Rehm et al., 2013). Their relation is depicted in Figure 13 below. The Reynolds number is calculated as:

$$Re = \frac{DU}{\nu_a} \quad (19)$$

where D is the diameter of the cylinder, for which the outer diameter of $0.565m$ is taken, and ν_a is the kinematic viscosity of air, for which a value of $1.45 \times 10^{-5}m^2/s$ is taken. By plugging the value obtained is $Re = 3 \times 10^5$. Considering the floater buoy to be a smooth surface, the value of $C = 0.7$ is obtained.

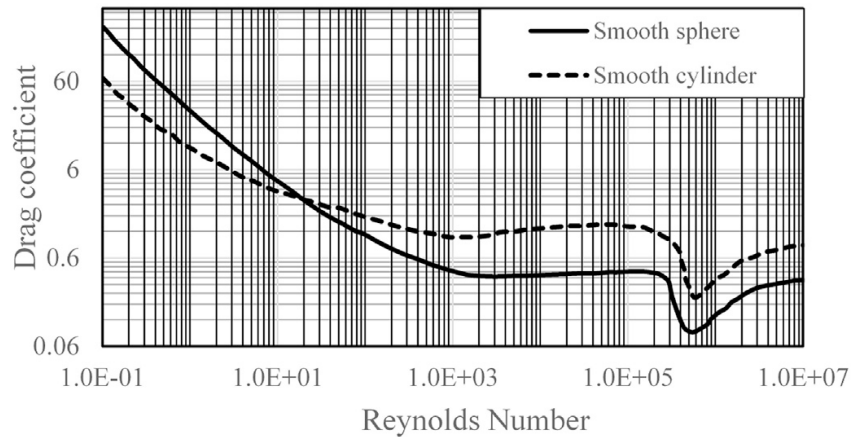


Figure 13: Drag coefficient for fixed circular cylinder and sphere for steady flow and smooth roughness (Schlichting and Gersten, 2000)

The area of the cylinder exposed to wind is the lateral surface above sea surface, calculated as $A = 2\pi Dh$. Plugging the values into Equation 18:

$$F_w = \frac{1}{2} \times 1.244 \text{kg/m}^3 \times 0.7 \times 0.5325 \text{m}^2 \times 7.8^2 \text{m/s} = 14.11 \text{N} \quad (20)$$

8.1.5 Current Force

Similarly to the mean wind force, the mean current force is calculated by means of the drag force equation:

$$F_c = \frac{1}{2} \rho_w C A U_c^2 \quad (21)$$

In this case, the density of seawater is considered, together with the mean current velocity U_c , taken to be 0.8m/s . Plugging in the previously computed values into the equation:

$$F_c = \frac{1}{2} \times 1027 \text{kg/m}^3 \times 0.7 \times 0.5325 \text{m}^2 \times 0.8^2 \text{m/s} = 122.5 \text{N} \quad (22)$$

8.2 Surge Displacement Analysis

A displacement analysis with respect to the environmental forces can be performed. Figure 14 shows the analytical approach from which the system will be studied. The environmental forces are denoted as F_{exc} , for excitation forces, corresponding to the wind, current and wave forces. Recall that these are obtained as mean values, except for the wave force, which depends on the incident wave height. Note that, as previously described, a still water level is considered at the testing harbour. For this reason, the wave force will only be considered as a force in the surge direction, neglecting the heave displacement Δz of the floater associated with this wave force. This can be seen as a theoretical assumption to study how the surge displacement varies with respect to a varying excitation force, while neglecting the associated heave displacement Δz . The following assumptions are considered for the static approach:

- The floater buoy is half-submerged at the initial position.
- The floater buoy geometry is approximated as depicted in Figure 12.
- The study is limited to 2 DOFs: surge and heave.
- The heave displacement Δz is neglected, given the still water level at the testing harbour.

- The forces incide on the floater in surge direction.
- The floater buoy does not sink as a consequence of surge displacement. The buoyancy force, therefore, remains constant.
- Tension forces are exerted on the outer sheath umbilical, thus neglecting the remaining umbilical components.
- The maximum tension occurs at the limiting case of the largest wave height, neglecting smaller wave sizes in between.

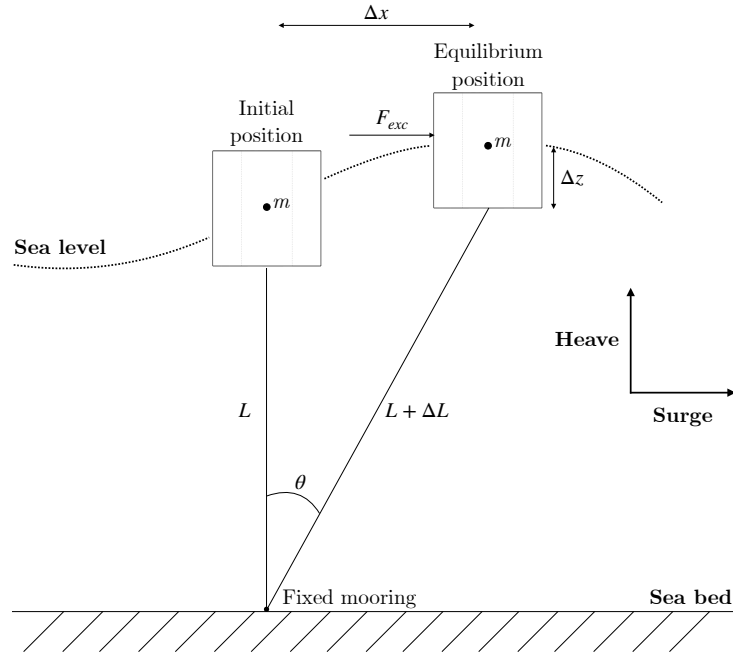


Figure 14: Static floater-cable system

Firstly, the initial position is examined, as depicted in Figure 15. At this instance, the forces acting on the cable are the net buoyancy force $F_{b,net}$ and the cable tension, denoted as F_{pre} for cable pretension. The net buoyancy can be computed as the buoyancy of the buoy minus its gravitational force:

$$F_{b,net} = F_b - F_g = 594.42N - 196.2N = 398.22N \quad (23)$$

Given equilibrium in the y-direction, the cable pretension F_{pre} is equal to the net buoyancy force, as $\sum F_y = 0$.

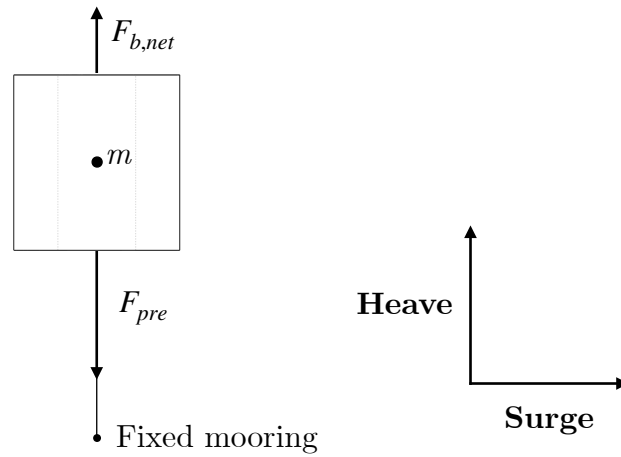


Figure 15: Static floater-cable system at initial position

When the force F_{exc} is applied on the buoy, the equilibrium position is reached. As depicted in Figure 14, the cable stretches by a length ΔL , resulting in a surge displacement Δx at an angle θ . This elongation is dependent on the stiffness of the umbilical cable k . Figure 16 depicts the forces acting at the equilibrium position. Notice that the net buoyancy force $F_{b,net}$ is not depicted in the free-body-diagram, as it is accounted for in the tension force T .

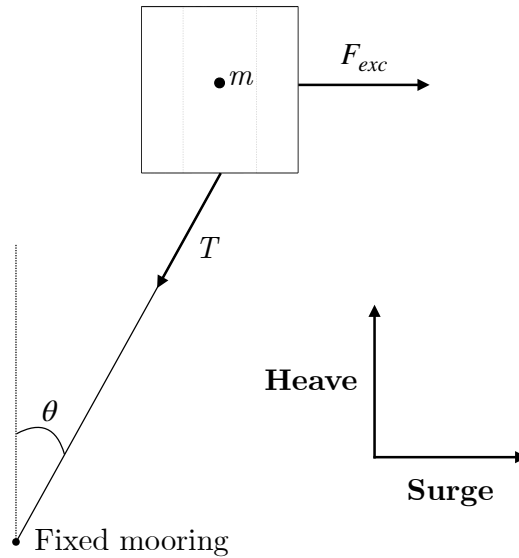


Figure 16: Static floater-cable system at equilibrium position

By examining the static equilibrium in the x-direction $\sum F_x = 0$:

$$T \sin \theta = F_{exc} \quad (24)$$

where the tension force T is the addition of the initial cable pretension F_{pre} and the elastic force F_k of the cable. Figure 17 represents the cable elongation and surge displacement at the equilibrium position.

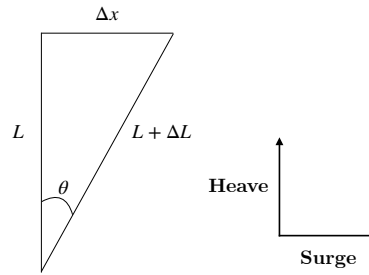


Figure 17: Elongation and surge displacement at equilibrium position

Using the Pythagorean theorem:

$$\sin\theta = \frac{\Delta x}{L + \Delta L} \quad (25)$$

Recall that the excitation force F_{exc} is the summation of the wave force and the mean wind and drift forces:

$$F_{exc} = F_{wind} + F_{current} + F_{drift} \quad (26)$$

Equation 24 can now be rewritten as:

$$(F_{pre} + F_k) \frac{\Delta x}{L + \Delta L} = F_{wind} + F_{current} + F_{drift} \quad (27)$$

The elastic force F_k , following Hooke's Law, is equal to the stiffness of the pipe k multiplied by the elongation of the pipe ΔL :

$$F_k = k\Delta L \quad (28)$$

ΔL is unknown, but is related trigonometrically to other variables, as can be deduced from Figure 17, yielding:

$$\Delta L = \sqrt{L^2 + (\Delta X)^2} - L \quad (29)$$

The spring constant k of the cable can be calculated theoretically. This is done by considering the cable as a straight beam with a fixed support on one end, and a force acting on the opposite end, as shown in Figure 18.

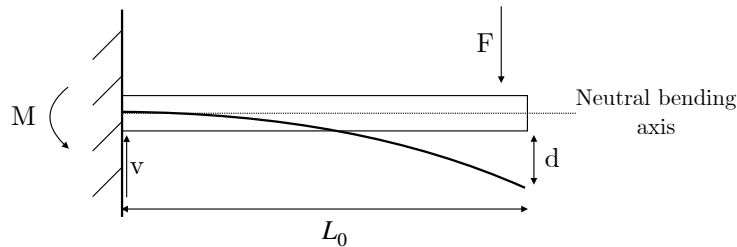


Figure 18: Deflection of straight beam

The deflection d of the straight beam is calculated as (Hibbeler, 2017):

$$d = \frac{FL_0^3}{3EI} \quad (30)$$

where F corresponds to the force applied F_{exc} , L_0 is the initial length of the umbilical, E is the Young's bending modulus with a value of $0.371GPa$ for PVC (Cambridge, 2014), and I is the moment of inertia. The moment of inertia for a straight circular beam is calculated as:

$$I = \frac{\pi}{64} (D_o^4 - D_i^4) \quad (31)$$

where D_o and D_i are the dimensions of the outer and inner diameters respectively. Plugging them into the equation, a moment of inertia of $I = 5.849 \times 10^{-6}m^4$. The equations can be rearranged in accordance with Hooke's Law:

$$F = k\Delta L \quad (32)$$

where ΔL is the deflection d of the beam. The elastic constant k can then be calculated by rearranging Equation 30 in terms of F and plugging it into Equation 32:

$$k = \frac{F}{d} = \frac{1}{\frac{L_0^3}{3EI}} = \frac{3 \times 0.371 \times 10^9 Pa \times 5.849 \times 10^{-6}m^4}{5^3m} = 52.079N/m \quad (33)$$

By plugging in these expressions into Equation 27, and substituting the previously calculated values for F_{wind} and $F_{current}$, and F_{drift} by Equation 17, the following expression is obtained:

$$\left[F_{pre} + k(\sqrt{L^2 + (\Delta X)^2} - L) \right] \frac{\Delta x}{\sqrt{L^2 + (\Delta X)^2}} = F_{wind} + F_{current} + \frac{1}{4}\rho_l g H^2 \quad (34)$$

This equation relates the wave height H and the surge displacement Δx . In Section 13, the relation between wave height and surge displacement will be presented.

8.2.1 Cable Pretension

The cable pretension is an important design parameter. On the one hand, the cable tension for the maximum force for the largest wave height cannot exceed the ultimate tensile strength (UTS) of the material. On the other hand, the larger the initial pretension of the cable, the less displacement of the buoy to the incident loads, and thus lower tension caused by the loads. It is then imperative to an optimal relation between these two factors. The maximum allowable load or cable tension can be derived from the UTS. The formula for stress is:

$$\sigma = \frac{F}{A} \quad (35)$$

where F is the tension acting perpendicular on the cable cross-section, and A the cross-sectional area of the cable. Substituting by the UTS for PVC (shown in Table 11), and by the area of the outer sheath of the material, the maximum allowable load can be computed:

$$F_{max} = 27.8 \times 10^6 Pa \times \frac{1}{4}\pi (0.0614^2 - 0.051^2) m^2 = 25523.153N \quad (36)$$

The perpendicular force component created by the excitation force F_{exc} must be calculated, and will be denoted as F_{\perp} . This load will vary with respect to the angle of displacement θ , as illustrated in Figure 19 below.

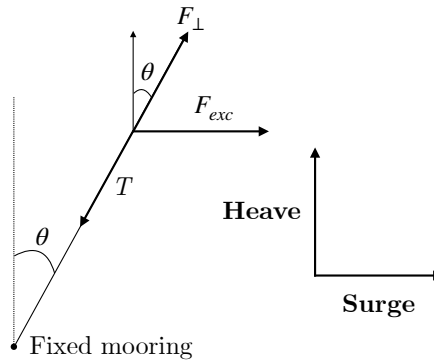


Figure 19: Variation of angular displacement and excitation force

For any given angular displacement θ , the perpendicular force can be obtained as:

$$F_{\perp} = \frac{F_{exc}}{\cos(90 - \theta)} \quad (37)$$

where θ is derived from Equation 25 to be:

$$\theta = \arcsin\left(\frac{\Delta x}{\sqrt{L^2 + (\Delta x)^2}}\right) \quad (38)$$

In order to not exceed the maximum allowable force F_{max} , the following condition must be met:

$$F_{pre} + F_{b,net} + F_{\perp} \leq F_{max} \quad (39)$$

MATLAB will be utilised as an optimisation problem solver. The following problem is set up:

Minimize obj. func. $F_{pre} + F_{b,net} + F_{\perp}$

with respect to:

Constraint 1: $c(1) = \Delta x - disp;$

Constraint 2: $c(2) = F_{pre} + F_{b,net} + F_{\perp} - F_{max};$

In essence, the objective function is to be minimized subject to two constraints. In MATLAB, constraints are set as values that must be less or equal to zero, that is, $c(1) \leq 0$ and $c(2) \leq 0$. The first constraint relates the surge displacement Δx to a maximum allowed displacement $disp$, which is an input variable. For the prototype umbilical, it is determined that the maximum displacement for the floater is at maximum 5 meters ($disp = 5$). Indeed, as $disp$ decreases, the lower the forces acting on the cable. The local minimum will thus always be located at $\Delta x = disp$. The second constraint sets all of the tension forces of the cable to be lower than the maximum allowable force. The optimization problem will be solved for the limiting condition, that is, for the maximum wave height of $h = 3$ meters. A brute force method for varying surge displacements can be used to solve the optimisation problem. In other words, the surge displacement will be decreased from the maximum surge value ($disp = 5$) to the point at which it converges to an unfeasible solution. The optimization scripts can be observed in Appendix C. These consist of three files: the main.m file of inputs and minimization options, the objective.m file for the objective function, and the nlcon.m function for non-linear constraints for the solver. To run the code, main.m is used as the executable file. Furthermore, the code in Appendix D was written to run the static analysis. The results will be presented in Section 13.

Part III

Full-scale Umbilical

9 Umbilical Cord

The full-scale umbilical solely serves the purpose of air pressurising. In essence, the cable equalises the pressures between the Ocean Battery reservoir and the sea surface. The operating depth ranges from 57 to 60 meters, due to tidal variation. This is a novel type of umbilical, as umbilicals in the renewable energy sector typically serve the purpose of electricity transmission or control and injection. This signifies a great engineering challenge, as the air ventilation hose is vulnerable to collapse under hydrostatic pressure. Existing literature and research on power umbilicals will be adapted to this specific application.

9.1 Umbilical Cross-section

Typical cross-sections of subsea power umbilicals are depicted in Figure 2 and Figure 20. It can be observed that the cable consists of an outer sheath material, followed by a layer of armouring, and a layer of inner sheath. Within these protective layers, the umbilical components for each specific application are contained. In this case, the inner part of the umbilical is a 54 cm ventilation hose, that is, an empty circular chamber.

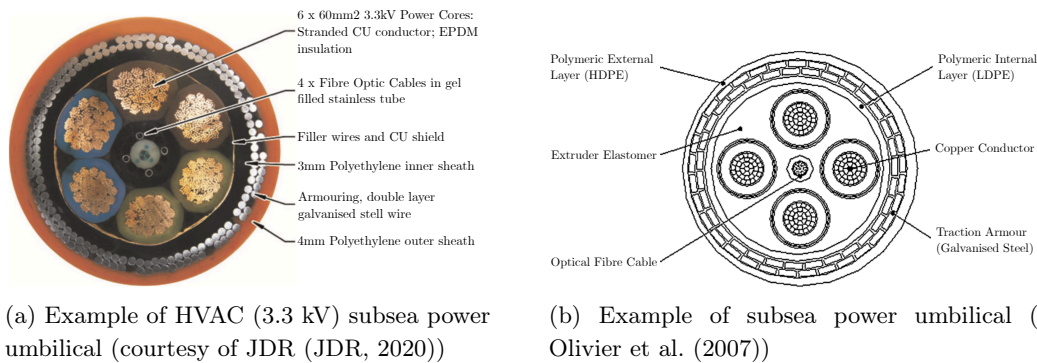


Figure 20: Typical cross-sectional structure of subsea power umbilical cables

Manufacturers tailor the subsea cable to the application at hand, implying that there is no such thing as a standardized cable. The subsea geometry of the cable will vary depending on the water depth and loading regimes (Clausen and D'Souza, 2001). The design characteristics and properties of the umbilical to consider are:

- The umbilical can withstand hydrostatic loading from underwater pressure.
- The umbilical can withstand forces from environmental loading from waves, wind and current.
- The umbilical is as light as possible, to reduce manufacturing costs.

9.2 Material Selection

The materials used in subsea power umbilicals appear to be consistent throughout literature: an outer sheath of either PE or HDPE, followed by an armouring layer of Galvanised Steel, and finally an inner sheath of either PE or HDPE. In reassurance, companies in the sector were approached. Fibron, a major designer, manufacturer and global provider of subsea cable and umbilical systems (Fibron, 2020), proposed employing a fibre braid layer instead of galvanised steel armouring. Secondly, the sales manager of JDR cables, a world-class provider of high performance subsea and

power cables (JDR, 2020), was contacted. Galvanised steel was recommended, and the above standard umbilical was provided (Figure 20(a)). Due to its properties and cost-effectiveness, galvanised steel will be selected as the armouring material for the umbilical. For the outer and inner sheath, HDPE will be again selected, for its beneficial properties in subsea applications.

9.3 Umbilical Design

The preliminary umbilical cross-section is depicted in Figure 21 below. In this project, the thickness of the outer and inner HDPE sheaths will be set at values of 4 and 3 cm respectively. This is due to the fact that their variation will not greatly affect the mechanical behaviour of the umbilical. The outer sheath serves the purpose of abrasion and collision protection. The inner sheath is a protective layer for the umbilical components contained in the umbilical. The thicknesses of these layers were obtained by up-scaling JDR's HVAC subsea power cable (Figure 20) to the required umbilical dimensions. In the same manner, the thickness of the galvanised steel layer would be 30 mm. This thickness will be used throughout the following sections, and will be given the name of 'reference thickness'.

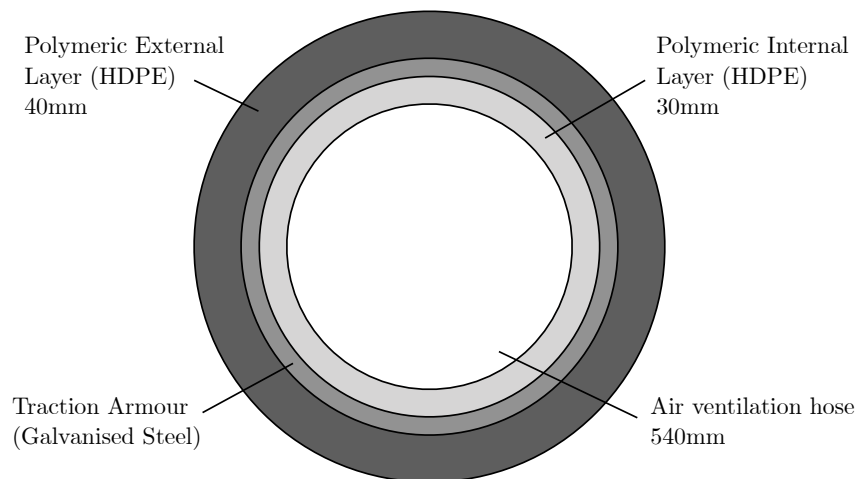


Figure 21: Preliminary umbilical cross-section

It is imperative to determine an optimal armouring sheath thickness. The thickness directly influences two critical design parameters: how much hydrostatic pressure the umbilical can withstand, and the overall weight of the umbilical and required buoyancy. At a density of $7850\text{kg}/\text{m}^3$, in comparison to HDPE's density of $958.5\text{kg}/\text{m}^3$, the amount of galvanised steel will directly impact the weight of the umbilical. This armouring consists of layers of helical strips of galvanised steel, and their cross-sectional design is critical. The number of layers must always be an even number, in which each layer of wires is set up in a different direction. This is due to the fact that steel strips are spiralled to form each wire, and will thus tend to create a torque in the helical direction on the umbilical. By opposing the direction of the layers, this torque is balanced.

10 Floater Buoy

A floater buoy that withstands the weight of the umbilical is to be designed. A similar design as the afore presented in Figure 10 will be adopted. In this case, the height will be set to 2 meters, the inner diameter to the diameter of the umbilical cable, and the outer diameter to the required buoyancy. The design directly depends on the thickness of the galvanised steel armouring layer.

This will determine both the diameter and weight of the umbilical. Moreover, the buoy will be designed with a buoyancy that enables it to be 25% out of the water (0.5 meters), to fulfil the purpose of air ventilation of the air hose. The material selected will once again be HDPE.

11 Analytical Calculations

A combination of methods will be utilised with respect to the previous static study (Section 8). In this case, the drift force from waves will be derived from the wave excitation forces obtained from NEMOH for an input buoy geometry. Moreover, the current force will be studied using Solidworks, and the wind force will still be calculated as a function of the exposed area of the buoy to wind. MATLAB will be utilised to relate the effect of different armouring layer thicknesses to the weight of the umbilical, desired buoy dimensions, and exerted wind and current forces.

11.1 Buoyancy Force

As previously explained, the required buoyancy force is dependent on the thickness of the outer sheath material. Appendix E shows the MATLAB script utilised to calculate the umbilical weight, and required buoy buoyancy, using the same procedure that was described in Section 8. The inputs to the program are the thicknesses of each umbilical layer. When using the reference value of 30 mm for the armouring layer, a buoyancy force of $F_B = 94468.452N$ is obtained, therefore requiring a buoy with a buoyancy of 9.63 tonnes. Various suppliers of heavy-duty HDPE buoys were analysed, and their buoys relevant for this application and with a buoyancy of 10 tonnes are gathered in Table 7.

Buoyancy (tonne)	Weight in air (tonne)	Product reference
10	1.8	APB-10000 (Fendercare, 2020)
10	1.7	APBB-10000 (Fendercare, 2020)
10	1.95	APB 10 (Telleborg, 2020)
12	2.72	Telemark (Telleborg, 2020)

Table 7: Types of buoys

By linearly approximating that a 10 tonnes Telemark buoy weighs 2.26 kg, the average mass of a 10 tonnes buoy can be calculated to be 1.9275 tonnes. This mass will be rounded up to 2 tonnes for ease in calculations. The equilibrium in the y-direction, for $\sum F_y = 0$, will determine the limit buoy volume to withstand the weight of the umbilical:

$$\rho_w V_{min} g = F_{b,required} + W_{buoy} \quad (40)$$

where $F_{b,required}$ is the calculated required buoyancy force to support the umbilical, and W_{buoy} is the weight of the buoy in Newton. Rearranging for the minimum volume required:

$$V_{min} = \frac{f_{b,required} + W_{buoy}}{\rho_w g} \quad (41)$$

Moreover, the volume of the buoy that is submerged is computed as:

$$V = \frac{1}{4} \pi (D_{outer}^2 - D_{umb}^2) h \quad (42)$$

where D_{outer} is the outer diameter of the buoy, D_{umb} is the diameter of the umbilical, and h is the depth of submersion of the buoy. The objective is to design a buoy that is 25 % above sea level. By setting the height of the buoy to 2 meters, and only varying the outer diameter of the buoy, this occurs when the buoy is 1.5 meters submerged. If the buoyancy equilibrium for a submersion of 1.5 meters is calculated, the optimal diameter of the buoy can be computed. That is, by setting $V = V_{min}$, $h = 1.5$, and solving for D_{outer} :

$$D_{opt} = \sqrt{\frac{V_{min} + \frac{1}{4}\pi \times 1.5D_{umb}^2}{\frac{1}{4}\pi}} \quad (43)$$

Yielding an optimal buoy volume of:

$$V_{opt} = \frac{1}{2}\pi (D_{opt}^2 - D_{umb}^2) \quad (44)$$

11.2 Wind Force

The wind force will be calculated in accordance with Equation 18. Once again, the geometry of the floater is cylindrical, and the shape factor C must be determined in accordance with Equation 19. For the reference value of a thickness of the armouring layer of 30mm, the Reynolds number is:

$$Re = \frac{D_{opt}U}{v_a} = \frac{6.1747m \times 7.8m/s}{1.45 \times 10^{-5}m^2/s} = 3.32 \times 10^6 \quad (45)$$

which corresponds to a drag coefficient $C=0.65$ (Figure 13). As the buoy geometry will not vary significantly for a different armouring thicknesses, a constant drag coefficient of $C=0.65$ will be assumed for varying thicknesses of the umbilical. The area exposed is half the lateral surface area above sea level:

$$A_{wind} = \frac{1}{2}\pi D_{opt}h \quad (46)$$

With every variable in Equation 18 known, the wind force can be computed. The MATLAB code in Appendix E allows to do so for a varying armouring layer thickness.

11.3 Wave Excitation Force

In this case, the BEM NEMOH will be used to calculate the wave excitation force, or drift force, on the buoy. As the body is symmetric, the contour of the buoy can be described with respect to an axis. This contour will be revolved around the axis by means of the `axiMesh.m` function in NEMOH. This is done for the various armour thicknesses, and the excitation forces obtained are gathered in Appendix J. The procedure will be demonstrated for the reference thickness ($t = 3cm$). The input geometry to the meshing code is the following array of radial and vertical coordinates, where the diameter of the buoy is computed through the MATLAB script in Appendix E.

```

1 clear all
2
3 n=5; % Number of points for discretisation
4 r=[ 0 6.1282 6.1282 0 0]; % Array of radial coordinates
5 z=[ 0.5 0.5 -1.5 -1.5 0.5]; % Array of vertical coordinates
6 [Mass,Inertia,KH,XB,YB,ZB]=axiMesh(r,z,n)
7 save('hydrostat_para', 'Mass', 'Inertia', 'KH', 'XB', 'YB', 'ZB')
```

Listing 1: Inputs for mesh generation

Input	Value
Number of points for angular discretization	100
Vertical position of gravity center	-0.5
Target for number of panels	1000

Table 8: Inputs to axiMesh.m function

Table 8 shows further inputs that are given to the axiMesh.m function. The center of gravity of the floater is at its center due to its symmetrical nature, and is thus located at $z = -0.5$ meters with respect to the water level. The output hydrostatic coefficients matrix is:

$$K_{h,s} = \begin{bmatrix} 0 & 0 & 0 & 0 & 0 & 0 \\ 0 & 0 & 0 & 0 & 0 & 0 \\ 0 & 0 & 1186141 & 0 & 9.7656 \times 10^{-4} & 0 \\ 0 & 0 & 0 & 10660020 & 0 & 0 \\ 0 & 0 & 9.7656 \times 10^{-4} & 0 & 10660020 & 0 \\ 0 & 0 & 0 & 0 & 0 & 0 \end{bmatrix} \quad (47)$$

Recall that the matrix specifies the variation of the net weight and buoyancy load with respect to the changes in position from equilibrium. For a hydrostatically stable body, the diagonal entries of the matrix must be positive. Indeed, this is the case for the designed floater, evidencing its stability. The output buoy discretisation and generated mesh are depicted in Figure 22 below. The axiMesh.m function creates a mesh considering the submerged surface of the buoy.

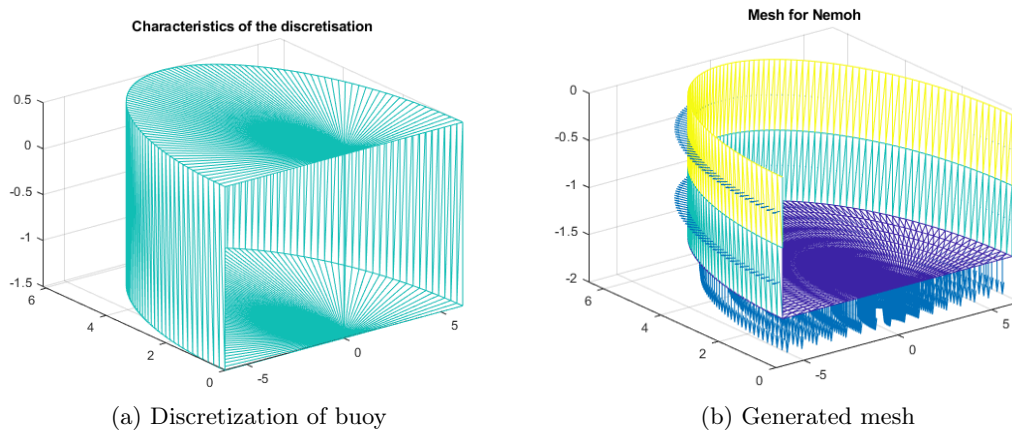


Figure 22: Discretisation and mesh of floater buoy

These meshes are utilised to run the NEMOH code. The wave characteristics are defined as shown in the code below. The frequency is defined to range from 0.1 to 20 rad/s, with a refinement of 0.1 rad/s. The wave direction is set to zero, which in NEMOH convention means that the waves incide in surge direction. Finally, the depth is set to 60 meters.

```

1 w= 0.1:0.1:20;           % Wave frequency [rad/s]
2 dir = 0;                 % Wave direction
3 depth=60;                % Water depth [m]
4 [A,B,Fe]=Nemoh(w, dir, depth)
5 save('hydrodyn_para', 'A', 'B', 'Fe')

```

Listing 2: Inputs for mesh generation

The excitation forces in 6 DOFs are obtained in the form of a matrix. These forces consist of real and complex parts. By plotting the absolute value of the excitation force in the surge direction against the wave frequency, the maximum force is calculated to be $273000N$, at a frequency of 1.4 rad/s.

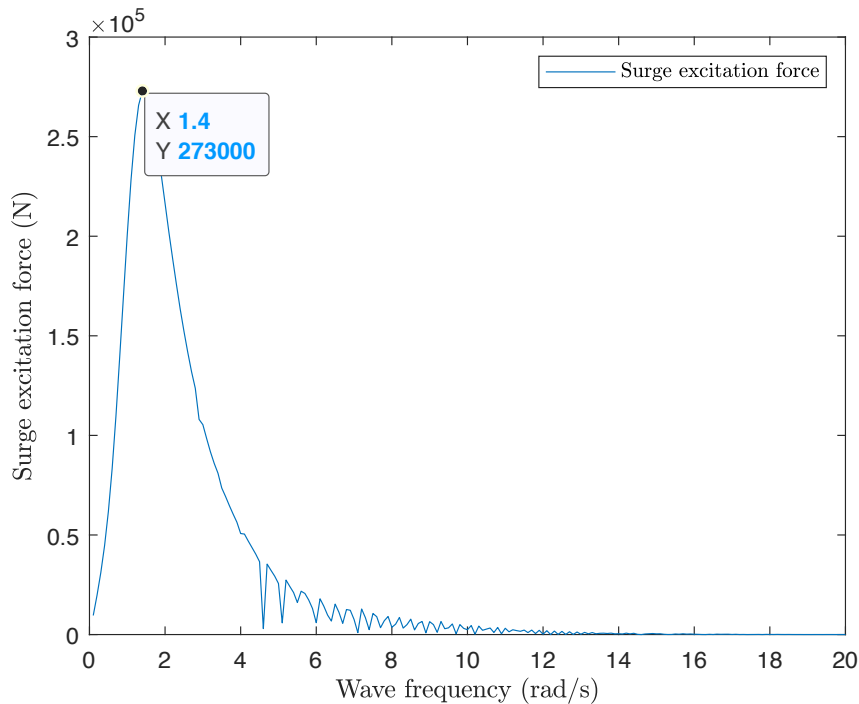


Figure 23: Surge excitation force plot for armouring thickness of 3 cm

11.4 Drag Force

The drag force opposes the excitation force from the incident wave. Recall from Equation 21 that it is dependent on the velocity of the flow around an object. In this case, the buoy can be considered to be stationary, with a wave inciding at a certain velocity, resulting in the excitation force. This velocity, or phase velocity v_p , is calculated as:

$$v_p = \frac{w}{k} \quad (48)$$

where w is the wave frequency (rad/s), and k is the wavenumber (rad/m). The wave number is calculated as:

$$k = \frac{2\pi}{\lambda} \quad (49)$$

where λ is the wavelength (m). The MATLAB script shown in Appendix F computes both the wave number and phase velocity for a given frequency and depth. Furthermore, the drag coefficient for

this geometry must now be determined. The Reynold's number, for the reference thickness of the armouring layer of $30mm$, is given by:

$$Re = \frac{D_{opt}U}{v_s} = \frac{0.74m \times 0.8m/s}{1.307 \times 10^{-6}m^2/s} = 4.529 \times 10^6 \quad (50)$$

The drag coefficient is defined to be $C_D = 0.6$, based on Figure 13. Once again, the drag coefficient will be assumed to be constant for varying thicknesses. The area exposed to the excitation force corresponds to the lateral surface of the cylinder submerged at a depth of $L = 1.5$ meters. This yields a lateral surface area of:

$$A_D = \frac{1}{2}\pi D_{opt} \times 1.5 \quad (51)$$

The terms will be plugged into the drag force equation for varying armouring thicknesses.

11.5 Current Force

The current force will be calculated in Solidworks Flow Simulation. As the umbilical is significantly larger than the floater buoy, the current force on the floater will be neglected. In Solidworks, the umbilical is subjected to a flow of water moving at the previously determined average velocity of 0.8 m/s. The Flow Simulation results will be translated into free-surface stress, and will be simulated alongside the other forces acting on the umbilical.

12 Simulation

In this section, the umbilical cord will be designed in Solidworks, and the forces and fixtures will be applied on it.

12.1 Umbilical Design

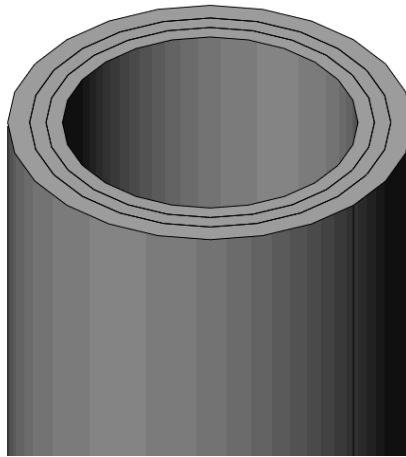


Figure 24: Amplified view of the umbilical open air hose

The umbilical is designed to be a 61.5 meter cylinder, with three layers of the aforementioned materials and a hollow 54 cm circular extrusion in its center. This is due to the fact that the system will be studied at the point where it is experiencing the maximum excitation force in surge direction. NEMOH generates a 1 meter amplitude wave, which generates the maximum excitation

force. The umbilical will then be 1 meter above still water level. Moreover, the umbilical will be inserted within the floater buoy, which will be designed to be 0.5 meters above sea level, for operational purposes. The umbilical cross-section is depicted in Figure 24 above.

12.2 Fixtures

The umbilical is fixed at the bottom surface. A simple fixture is considered, and the surfaces of the three layers are used as fixtures. Appendix G describes the fixtures and meshing applied in Solidworks in further detail.

12.3 Loads

12.3.1 Ocean Pressure

The hydrostatic loading from the ocean pressure is applied on the submerged part of the umbilical. The part of the umbilical that is within the buoy is not included, as the buoy itself will be withstanding the pressure. The pressure is applied as a function of the depth below sea level. For this purpose, a reference coordinate system is generated at the end of the umbilical. The following pressure function is used:

$$P = \rho_w g (y - 2) \tag{52}$$

where y is vertical displacement in meters with respect to the reference coordinate system. Note that $y - 2$ is to solely consider the part of the umbilical that is not inside the buoy. This creates a pressure gradient, with increasing pressure the lower beneath the sea surface. Figure 25 depicts the resulting load.

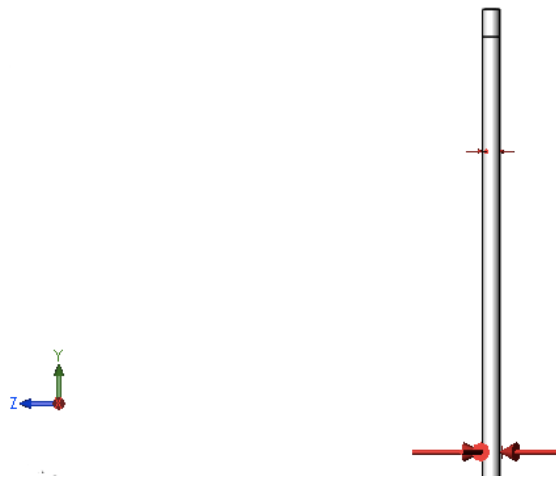


Figure 25: Surface flow plot of current load

12.3.2 Current Force

The Solidworks Flow Simulation tool is utilised to study the drag force from the mean ocean current. An external study is run, to study the fluid acting on the outside of the umbilical. Water is selected as the desired fluid, and is set to be moving at the mean velocity value of 0.8 m/s in the negative z-direction. The outcome in terms of pressure is depicted in Figure 26 and Figure 27, in the form of surface and contour plots respectively. These results will be translated into free-surface stress, and applied alongside the remaining loads in a simulation.

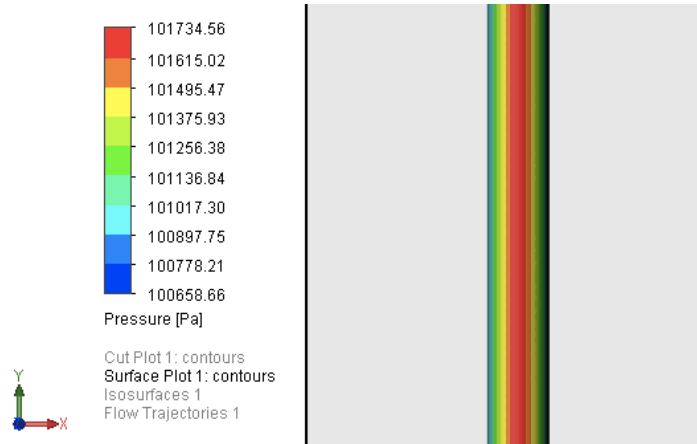


Figure 26: Surface flow plot of current load

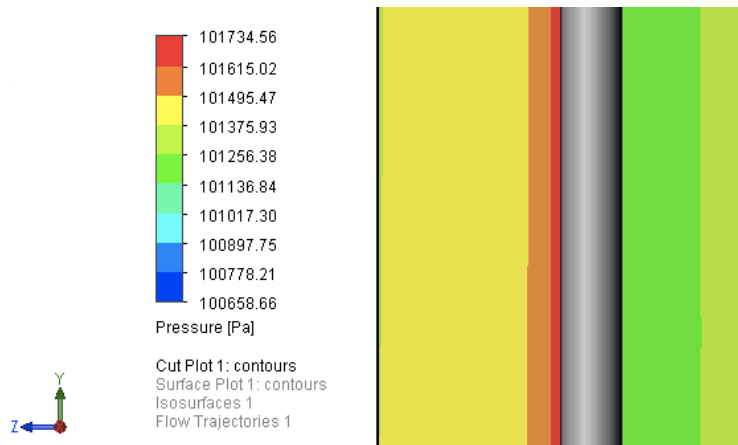


Figure 27: Contour plot of current load

12.3.3 Wave Excitation and Wind Force

The wave excitation force is applied on the top 2 meter part of the umbilical, where the buoy would be inserted, in the negative z-direction. The wind force is also applied in the same direction and surface. With the drag force acting against the wave excitation force in the positive z-direction, the resultant force to be applied is:

$$F_{resultant} = F_{exc} + F_{wind} - F_D \quad (53)$$

The force is applied as depicted in Figure 28.

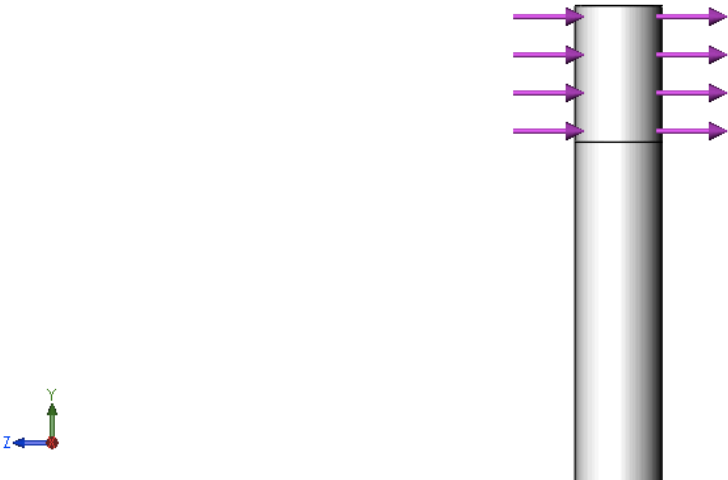


Figure 28: Resultant excitation force

Figure 29 displays the umbilical with the fixtures and loads applied on it. Notice that the current force is not considered as a load. Solidworks translates the Flow Simulation results into fluid shear stress when importing the results into the simulation, but are not depicted as a force.



Figure 29: Isometric view of loads and fixtures applied on the umbilical in Solidworks

13 Results

13.1 Analytical Static Analysis

The optimal umbilical pretension can be determined for a varying range of allowable displacement $disp$. By a brute force method approach, the minimum allowable displacement was found to be at $\Delta x = 3.3125$ meters. Table 9 below gathers the outputs of optimal pretension (F_{pre}), constraint 1 ($cq.1$) and constraint 2 ($cq.2$) for a varying range of surge displacements. Moreover, the Factor of Safety was calculated as follows

$$FOS = \frac{F_{max}}{F} = \frac{F_{max}}{F_{max} - cq.2} \quad (54)$$

As the second constraint, $cq.2$, is the additional force that must be added to reach the maximum allowable force, F can be computed as $F_{max} - cq.2$

Δx	F_{pre}	cq. 1	cq. 2	FOS
3.0625	12505.816	0	-68.460	1
3.25	11978.400	4.3472e-11	1118.091	1.046
3.5	11373.892	1.0028e-12	2319.846	1.1
3.75	10860.677	-4.4409e-16	338.657	1.15
4	10420.820	-4.4409e-16	-4210.418	1.198
4.25	10040.649	1.0355e-9	-4962.496	1.241
4.5	9709.572	5.5067e-14	-5616.100	1.282
4.75	9419.266	8.5555e-11	-6187.895	1.32
5	9163.120	6.8268e-19	-6691.44	21.355

Table 9: Results

MATLAB approximates the outputs of $cq.1$ to zero, due to being infinitesimally small numbers, and thus considering the solutions for F_{pre} to be feasible. A choice of F_{pre} must be made in accordance to the desired surge displacement and related FOS. These are plotted in Figure 30 below.

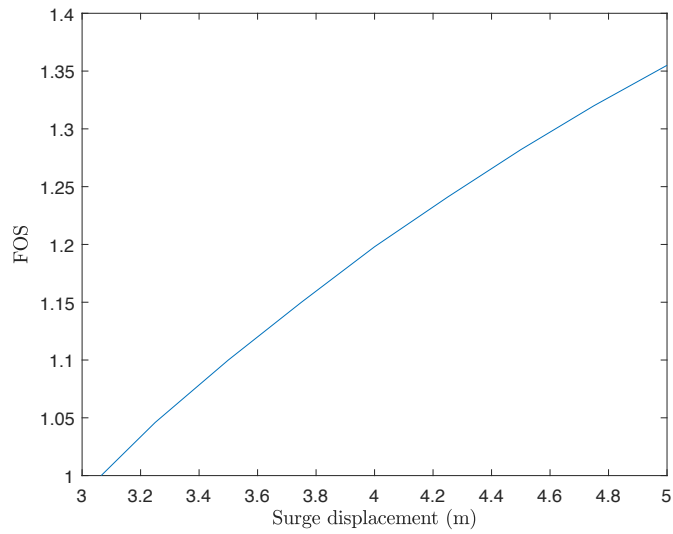


Figure 30: Factor of safety for varying surge displacement

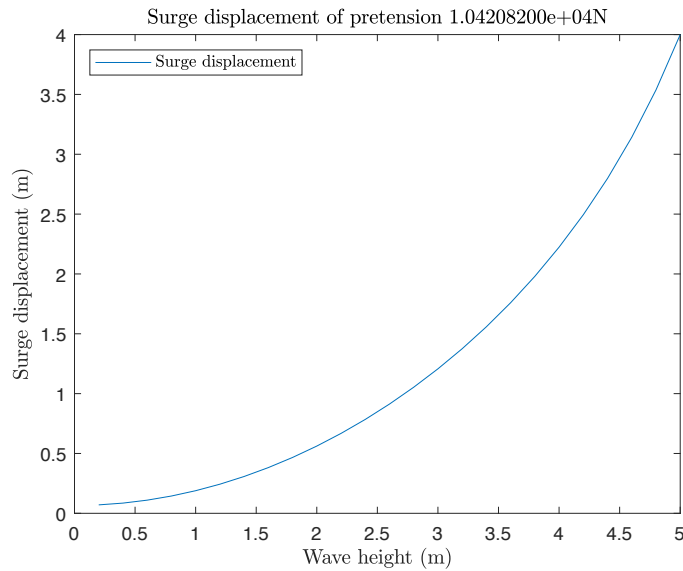


Figure 31: Surge displacement for $F_{pre} = 10420.820N$. Maximum displacement $\Delta x = 4m$

It can be observed that the surge displacement increases exponentially for the input wave height.

13.2 Simulation Static Analysis

The von Mises Stress, FOS and surge displacement was simulated for varying armouring thicknesses. The results are gathered in Table 10 below. These values were obtained by running simulations on Soliworks. The wave excitation forces for each thickness can be observed in Appendix J. The MATLAB script in Appendix E was further utilised to calculates the resultant force to apply on Soliworks. Furthermore, Appendix K shows Solidworks FOS, surge displacement and von Mises stress simulation results.

Thickness (cm)	D_{opt} (m)	F_{exc} (N)	w (rad/s)	v (m/s)	F_R (N)	Max von Mises (Pa)	Min FOS	Surge displacement (m)
2.5	5.7230	251900	1.4	7.5007	17837.345	$2.219e + 8$	0.899	3.250
2.75	5.9523	262700	1.4	7.5007	19258.391	$1.725e + 8$	1.121	3.003
3	6.1747	273000	1.4	7.5007	20459.613	$1.543e + 8$	1.133	2.879
3.25	6.3911	282600	1.4	7.5007	21211.751	$1.598e + 8$	1.188	2.75
3.5	6.6019	291700	1.4	7.5007	21690.138	$1.541e + 8$	1.270	2.753
3.75	6.8077	300400	1.4	7.5007	21973.754	$1.165e + 8$	1.674	2.135
4	7.0089	308600	1.4	7.5007	21944.523	$1.165e + 8$	1.674	2.135
4.25	7.2059	316500	1.4	7.5007	21786.767	$1.058e + 8$	1.812	1.997
4.5	7.3991	324000	1.4	7.5007	21386.787	$9.339e + 7$	2.028	1.657
4.75	7.5887	328500	1.4	7.5007	18132.535	$7.791e + 7$	2.283	1.376
5	7.7749	335300	1.4	7.5007	17313.350	$7.001e + 7$	2.697	1.205
5.25	7.9582	341900	1.4	7.5007	16419.747	$6.277e + 7$	2.917	1.077

Table 10: Results for varying armouring layer thickness

It can be observed that the FOS increases linearly with the thickness of the armouring layer. Moreover, this determines the overall weight of the umbilical, and thus the buoyancy force required. Figure 32 shows a plot of the FOS against the required buoyancy. The results will be further discussed in Section 14.

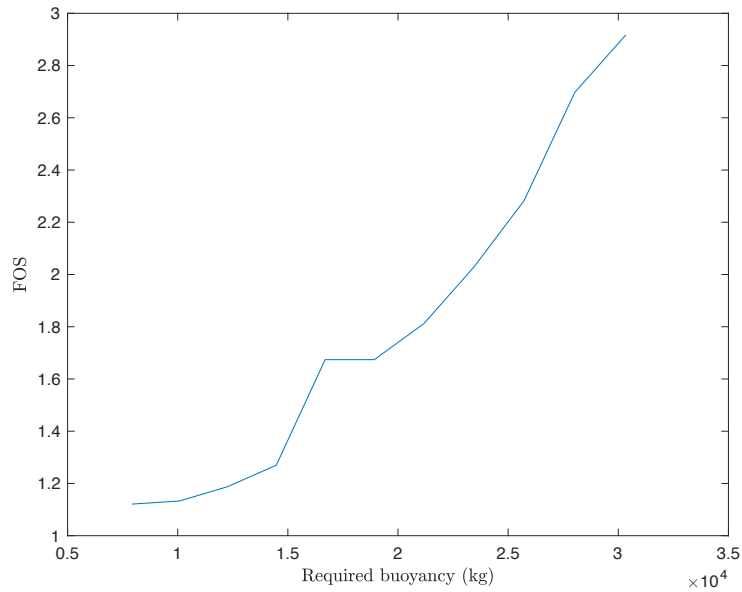


Figure 32: Plot of FOS against required umbilical buoyancy (kg)

14 Discussion

In this section, the obtained results will be discussed, and a selection of a feasible FOS for each analysis will be selected. Finally, the limitations of these studies will be discussed, together with further research.

14.1 Results Discussion

There are two key considerations when selecting a feasible FOS: the associated costs, and the structural failure of the system or structure. On the one hand, a larger FOS will result in either operational costs, in terms of the allowable surge displacement of the prototype umbilical, or associated costs, in terms of the amount of raw material that is required for both the umbilical and floater buoy. On the other hand, a FOS of at least 1 is required for the umbilical to withstand environmental loading. In the first study concerning the prototype umbilical, the system is to be operating for a limited amount of time, thus neglecting the deterioration of the cord over time. Moreover, it will operate at a testing harbour under steady water conditions. For this reason, any FOS above 1 is considered optimal. For instance, a maximum surge displacement of 4 meters, with an optimal cable pretension of $F_{pre} = 10420.820N$ and FOS of 1.198, is deemed sufficient. In essence, this study corroborates the structural advantages of PVC as an outer sheath material. Despite the plain water surface at the testing harbour, the umbilical shows to withstand loading from wave drift force from wave amplitudes of up to 3 meters.

For the full-scale umbilical, an armouring thickness of 3cm, for which a FOS of 1.133 ensured, will be considered optimal. The simulations were run for the limiting case scenario, at which the loads are applied in the same direction and the maximum wave excitation force is studied. Despite considering average wind and current loads, their variation showed little effect on the structural integrity of the system. Conversely, the wave excitation force greatly impacts the stability of the system. This, together with assumptions such as the simple buoy geometry and Ocean Battery connection, deem a FOS of 1.133 feasible, and will be further discussed in the following section.

14.2 Limitations

Significant assumptions have governed both studies, and will limit the usefulness of the results. In the first study, the heave displacement, together with the sinking of the buoy when being displaced and moored, were neglected. Realistically, wave excitation loading will be present in both the heave and surge direction. Moreover, despite the outer sheath withstanding a displacement of 4 meters with a FOS of 1.198, the umbilical components will likely fail under these conditions. For operational purposes, it is unfeasible to be elongated to a surge displacement of 4 meters. In essence, the study was a large approximation of environmental loading on the system.

On the contrary, the second static analysis was a closer representation of reality, while still considering notable assumptions. Namely, the mass of the buoy was approximated, the buoy geometry was considered to be simple, the heave excitation force was not considered, and the Ocean Battery connection was not studied. Firstly, the average value from buoys with a buoyancy of 10 tonnes was taken, as it was initially determined to be the approximated weight by up-scaling the dimensions of smaller subsea umbilicals. This assumption reflects the validity of the results obtained, making armouring thicknesses with a required buoyancy close to 10 tonnes more accurate. Secondly, the buoy was considered to be a cylinder, in which the floater height was set at a constant value, for the ease of running multiple simulations. For the same reason, the drag coefficient was set to a constant value of $C_D = 0.6$. Further consideration must be paid to the geometry of the buoy, as it will greatly determine the associated wave excitation force. Thirdly, the study did not consider excitation in the heave direction, making it strictly a surge displacement analysis, and not studying the full range of motion of the system. Finally, the Ocean Battery connection was

considered to simply be represented as a fixture of the cross-sectional surface of the umbilical. The maximum stress was observed to occur at this location. Different connection points, such as a flange connection, will decrease stress, as the same force will be distributed over a larger surface. The selection of an armouring thickness of 3 centimetres, despite a seemingly low FOS (1.33), is an estimate of the optimal umbilical thickness. On the one hand, detailed buoy design will decrease the wave excitation force on the umbilical. Furthermore, the design of an Ocean Battery connection point will reduce stress concentration, thus increasing the FOS. On the other hand, a buoyancy of 10.09 tonne is required for a thickness of 3 centimetres, making the result accurate in terms of the assumption on the mass of the buoy.

14.3 Further Research

Initially, this project aimed to perform a dynamic study on the response of the floater-umbilical system to environmental loading. The open-source code Wec-Sim was utilised, and run in MATLAB to simulate the floater buoy. Furthermore, a second open-source code, Moordyn, would implement a lumped-mass approach to simulate the umbilical cable as a mooring line for the buoy. Shortcomings were found through this approach. The desired umbilical geometry was not able to be designed, as the air ventilation hose and three outer sheath layers could not be extruded. Further research from a dynamic approach is encouraged, likely utilising a different software. The aforementioned assumptions would be accounted for, together with including the inertia of the added mass and the viscosity of the surrounding fluid, which could not be included in this static analysis. Furthermore, the floater geometry, and the effects of different shaped buoys, should be accounted for in further research in the field. Moreover, research into the cross-sectional layout of the umbilical is recommended. Instead of containing a large air-ventilation hose, the umbilical could consist of various smaller hoses. A filler material would be included between the hoses, making the umbilical less vulnerable to environmental loading. Finally, research on the Ocean Battery connection is required.

Conclusion

Environmental loading from waves, wind, and currents has been identified as an undermining factor of the structural integrity of offshore systems. An initial analytical attempt to model environmental loading on a prototype floater-umbilical system was performed. An optimisation surge displacement problem was set up, to model the static response of the prototype umbilical cord to hydrostatic loading in terms of cable force and displacement. It was found that the cable pretension and surge displacement were strictly related, together with the FOS of the system. A FOS of 1.198 was obtained, for a cable pretension of 104030.820N and surge displacement of 4 meters. However, it must be concluded that this study does not serve as an accurate surge displacement analysis, due to the significant assumptions governing it. However, given the still water conditions at the testing harbour, the study serves to portray the advantages of PVC as an outer sheath material, as it showed to withstand loading from waves in up to 5 meter amplitude. It can be concluded that PVC is a feasible material for the small-scale harbour test. Moreover, a floater buoy was designed for such an application. With a dominating position in the industry due to its many excellent properties, cost-effectiveness, and ease of fabrication, HDPE was selected as an optimal floater buoy material. The floater buoy geometry was discussed, and a ‘two shell’ floater buoy was designed for such an application.

Secondly, a feasible design for the outer sheath layers of the full-scale umbilical was determined. The umbilical designed consists of a 4 centimetres outer sheath of HDPE, followed by a 3 centimetre galvanised steel armouring layer, and by a 3 centimetre inner sheath layer of HDPE. Indeed, the outer and inner sheath layers showed little effect in the mechanical behaviour of the cable under hydrostatic loading. The outer sheath layer solely serves the purpose of abrasion and UV resistance, while the inner layer serves the purpose of protection of the armouring layer from corrosion. The umbilical design was validated analytically in Solidworks, and experimental validation is yet to be performed. However, the dimensions of the umbilical are consistent with upscaling a subsea power cable by JDR. This design ensures a FOS of 1.133, which was discussed to be sufficient due to simplifications of the buoy geometry, and consideration of the limiting case scenario. The excitation force in surge direction caused by waves of unity amplitude was calculated by means of NEMOH. At the frequency for maximum excitation, the resulting surge displacement was 2.879 meters. The weight in air of the designed umbilical is 37034.737 kilograms, and will require a buoyancy of 10 tonnes for operational purposes. Overall, the thickness of the armouring sheath was observed to be a key parameter to stabilise the floater-umbilical system against environmental loading.

In essence, this research took a first step towards designing the full-scale floater-umbilical system for its deployment in open-sea. Significant assumptions governed this study, thus limiting the validity of the outcome of this research, and requiring further research. In particular, it is imperative that the system is studied from a dynamic approach, with further attention to the effects of varying buoy geometry, the Ocean Battery connection point, and umbilical cross-sectional layout.

Bibliography

- (2012). North sea climate. *Climate Data*. Available at <https://en.climate-data.org/north-america/united-states-of-america/new-york/north-sea-141630/>.
- (2016). Fossil fuels. *Environmental and Energy Study Institute*. Available at <https://www.eesi.org/topics/fossil-fuels/description#:~:text=According%20to%20the%20U.S.%20Energy,changes%20in%20the%20Earth's%20climate>.
- (2018). Do renewable energy technologies need government subsidies? *The London School of Economics and Political Science*. Available at <http://www.lse.ac.uk/GranthamInstitute/faqs/do-renewable-energy-technologies-need-government-subsidies/>.
- (2019). Cat 6a interactive reference guide. *Leviton*. Available at https://www.leviton.com/en/docs/Leviton_Cat6AReferenceGuide.pdf.
- (2019). Tubing & hose metric. *Norgren*. Available at <http://www.farnell.com/datasheets/20632.pdf>.
- (2019). Umbilicals. *Subseapedia*. Available at <http://www.subseapedia.org/w/index.php?title=Umbilicals>.
- (2019). Wec-sim theory. *Github*. Available at <https://wec-sim.github.io/WEC-Sim/theory.html#id4>.
- (2020). Air - density, specific weight and thermal expansion coefficient at varying temperature and constant pressures. *The Engineering Toolbox*. Available at https://www.engineeringtoolbox.com/air-density-specific-weight-d_600.html.
- A. Nesegard, M. Ronaess, O. H. K. R. and Bitner-Gregersen, E. M. (2010). Dnv-rp-c205: Environmental conditions and environmental loads. page 124.
- Ammalaa, A., Batemana, S., Deana, K., Petinakis, E., Sangwan, P., Wonga, S., Yuana, Q., Yua, L., Patrickb, C., and Leongb, K. (2010). An overview of degradable and biodegradable polyolefins. *Progress in Polymer Science*, 36:1015–1049.
- Bai, Y. and Bai, Q. (2012). *Subsea Engineering Handbook*. Gulf Professional Publishing.
- Beirão, P. and Malça, C. (2014). Design and analysis of buoy geometries for a wave energy converter. *International Journal of Energy and Environmental Engineering*, 5:1–11.
- Brent, M. (2019). Differences between polyethylene and polyurethane. *Sciencing*. Available at <https://sciencing.com/differences-between-polyethylene-polyurethane-8514564.html>.
- Cambridge (2014). Cambridge engineering selector granta (ces edupack material level 3).

- Chang, H.-C. and Chen, B.-F. (2019). Mechanical behavior of submarine cable under coupled tension, torsion and compressive loads. *Ocean engineering*, 189.
- Clausen, T. and D'Souza, R. (2001). Dynamic risers key component for deepwater drilling, floating production. *Offshore*, 61(5):89–92.
- Coelingh, J., [van Wijk], A., and Holtslag, A. (1996). Analysis of wind speed observations over the north sea. *Journal of Wind Engineering and Industrial Aerodynamics*, 61(1):51 – 69.
- Faltinsen, O. (1993). *Sea loads on ships and offshore structures*, volume 1. Cambridge university press.
- Feldman, D. (1984). Weathering of polymers, a. davis and d. sims, applied science publishers, london, 1983, 294 pp. price: \$64.75. *Journal of Polymer Science: Polymer Letters Edition*, 22(7):423–423.
- Fendercare (2020). Fendercare: Flotation and buoyancy. *Fendercare Marine*. Available at https://www.fendercare.com/files/6314/8794/3718/Flotation_Buoyancy_LR.pdf.
- Fibron (2020). Fibron: Renewable energy cables. *Fibron*. Available at <https://fibron.com/product/renewables-tidal-and-wind/>.
- Fonseca, N., Pascoal, R., Marinho, J., and Morais, T. (2008). Analysis of wave drift forces on a floating wave energy converter. volume 6.
- Granqvist, C. (2003). Solar energy materials. *Advanced Materials*, 15(21):1789–1803.
- Hibbeler, R. (2017). Statics and mechanics of materials, 5th global ed.
- JDR (2020). Jdr: Renewable energy. *JDR*. Available at <https://www.jdrcables.com/renewables/>.
- Kersten, I. A., Kornilova, E. V., and Michailov, A. A. (2019). Finite element definition of effective stiffness coefficients for power submarine cable with heterogeneous structure. *Marine Intellectual Technologies*, 3(3):208–215.
- Khan, D. and Ulucak, R. (2020). How do environmental technologies affect green growth? evidence from brics economies. *Science of The Total Environment*, page 136504.
- Martinelli, L., Lamberti, A., Ruol, P., Ricci, P., Kirrane, P., Fenton, C., and Johanning, L. (2010). Power umbilical for ocean renewable energy systems-feasibility and dynamic response analysis.
- Olivier, N., Machado, I., and Goncalves, E. (2007). Cyclic loading and marine environment effects on the properties of hdpe umbilical cables. *Journal of Materials Science*, 42:6935–6941.
- Patel, H. (2008). Subsea umbilicals and power cables.steege lecture 44. *STEEGE Lecture 44*.
- PIPA (2016). Industry guidelines pop202: Pvc, pp and pe pipe installation on curved alignments. *Plastics Industry Pipe Association of Australia Limited*, 2(1).
- Platzer, N. (1986). Encyclopedia of polymer science and engineering, h. f. mark, n. m. bikales, c. g. overberger, and g. menges, wiley-interscience, new york, 1985, 720 pp. *Journal of Polymer Science Part C: Polymer Letters*, 24(7):359–360.
- Rehm, B., Haghshenas, A., Paknejad, A. S., Al-Yami, A., and Hughes, J. (2013). *Underbalanced drilling: limits and extremes*. Elsevier.

- Rentschler, M. U., Adam, F., Chainho, P., Krügel, K., and Vicente, P. C. (2020). Parametric study of dynamic inter-array cable systems for floating offshore wind turbines. *Marine Systems & Ocean Technology*, 15(1):16–25.
- Sahu, A. (2017). Effect of uv exposure on bimodal hdpe floats for floating solar application. *Journal of Materials Research and Technology*, 8.
- Sahu, A., Sudhakar, K., and Sarviya, R. (2019). “influence of u.v light on the thermal properties of hdpe/carbon black composites.”. *Case Studies in Thermal Engineering*, 15:100534.
- Sahu, A., Yadav, N., and Sudhakar, K. (2016). Floating photovoltaic power plant: A review. *Renewable and Sustainable Energy Reviews*, 66:815 – 824.
- Schlichting, H. and Gersten, K. (2000). *Boundary-Layer Theory*. Springer.
- Telleborg (2020). Telleborg: Product brochure. *Trelleborg Marine and Infrastructure*. Available at <https://www.trelleborg.com/en/marine-and-infrastructure/products--solutions--and--services/marine/surface--buoyancy/mooring--buoys/mooring--buoy>.
- Thies, P. R., Johanning, L., and Smith, G. H. (2012). Assessing mechanical loading regimes and fatigue life of marine power cables in marine energy applications. *Proceedings of the institution of mechanical engineers part o-journal of risk and reliability*, 226(O1, SI):18–32.
- Wei, Y., Yu, Z., Barradas Berglind, J., van Rooij, M., Prins, W., Jayawardhana, B., and Vakis, A. (2017). A frequency-domain model for a novel wave energy converter. In *European Wave and Tidal Energy Conference Series (EWTEC)*.
- Worzyk, T. (2009). Submarine power cables: design, installation, repair, environmental aspects. *Submarine power cables*.
- Yang, S.-H., Ringsberg, J. W., and Johnson, E. (2018a). Parametric study of the dynamic motions and mechanical characteristics of power cables for wave energy converters. *Journal of marine science and technology*, 23(1):10–29.
- Yang, Z., Lu, Q., Yan, J., Chen, J., and Yue, Q. (2018b). Multidisciplinary Optimization Design for the Section Layout of Umbilicals Based on Intelligent Algorithm. *Journal of offshore mechanics and arctic engineering-transactions of the ASME*, 140(3).

Appendices

A Material Properties

A.1 Polyvinyl Chloride (PVC)

Composition Overview		Production Recyclability	
Base	Polymer	CO2 primary production	58.3 MJ/kg
Polymer Class	Thermoplastics: amorphous	Water usage primary production	207.5 l/kg
Polymer type	PVC	CO2 polymer extrusion	0.452 kg/kg
Polymer full name	Polyvinyl chloride, rigid, unplasticised	CO2 polymer molding	1.265 kg/kg
Filler type	Unfilled	Processing Properties	
Price	1.11 EUR/kg	Polymer injection molding	Acceptable
Density	1310 kg/m ³	Polymer extrusion	Excellent
Material Properties		Durability	
Young's Modulus	0.371 GPa	Water (fresh)	Excellent
Yield strength	30.6 MPa	Water (salt)	Excellent
Tensile strength	27.8 MPa	Weak acids	Excellent
Elongation	200 % strain	Strong acids	Acceptable
Elongation at yield	22.5 % strain	Weak alkalis	Excellent
Compressive modulus	0.371 GPa	Strong alkalis	Acceptable
Flexural modulus	0.55 GPa	Organic solvents	Unacceptable
Flexural strength	17.89 MPa	Oils and fuels	Limited use
Shear modulus	0.12 GPa	Oxidation at 500C	Unacceptable
Shear strength	22.5 MPa	UV radiation	Good
Poisson's ratio	0.435	Flammability	Slow-burning

Table 11: PVC (Semi-rigid, molding and extrusion) properties (Cambridge, 2014)

A.2 High-density Polyethylene (HDPE)

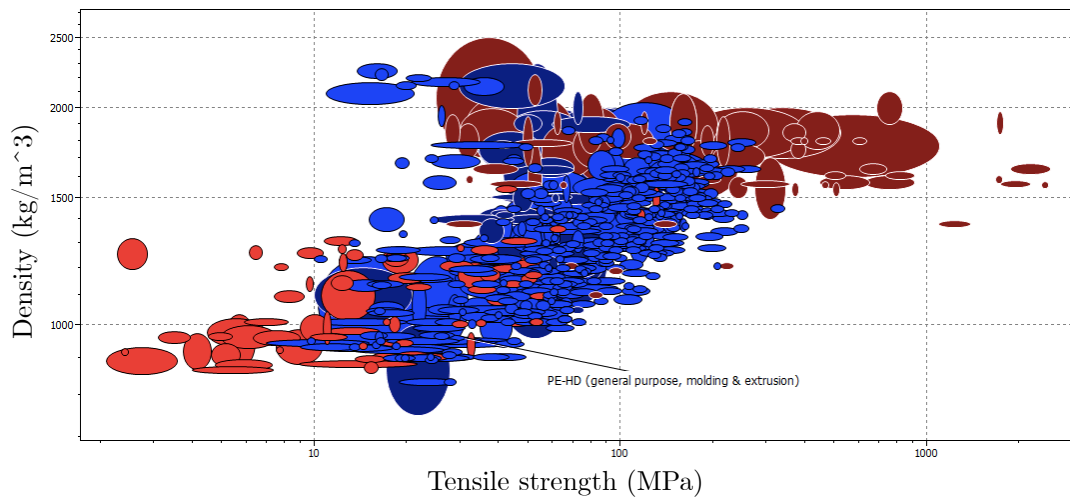


Figure 33: Tensile strength (MPa) against density (kg/m^3)

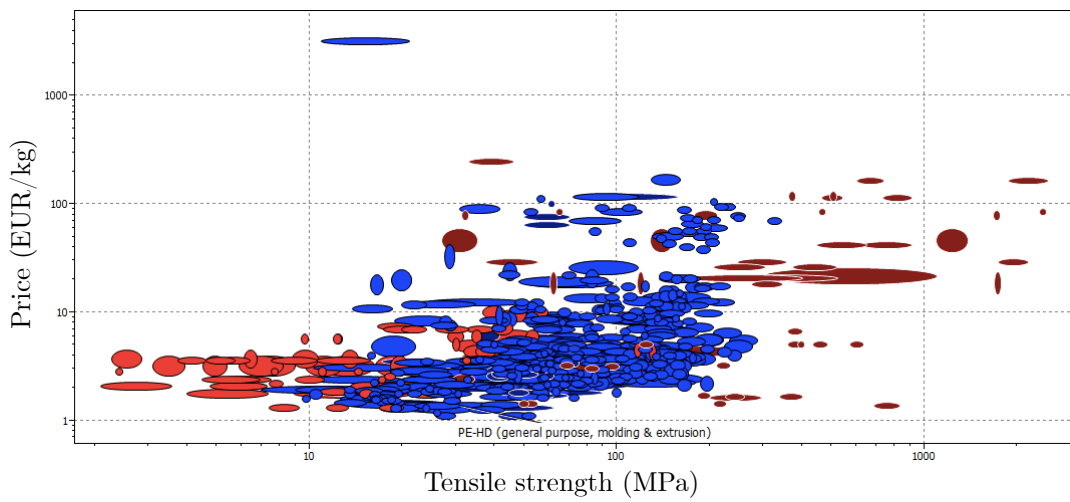


Figure 34: Tensile strength (MPa) against price (EUR/kg)

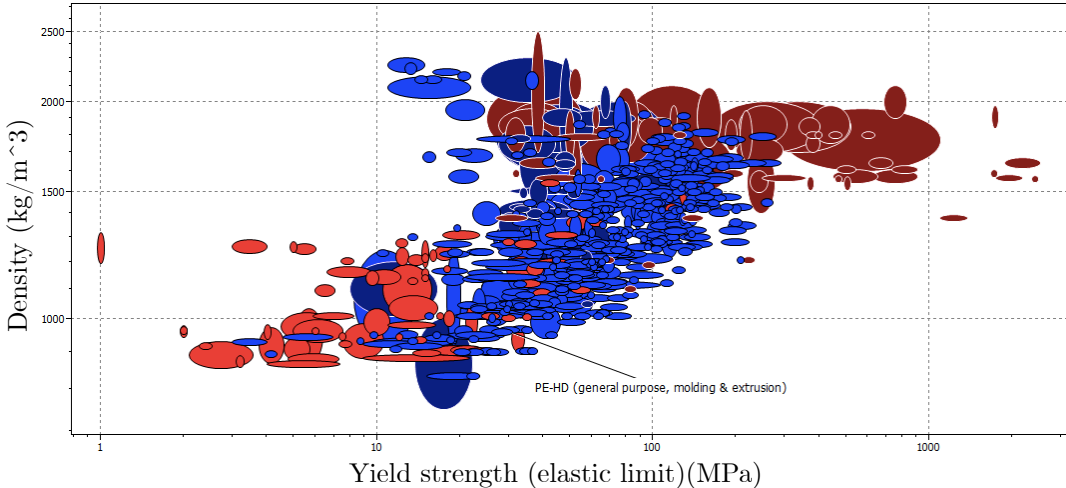


Figure 35: Yield strength (elastic limit)(MPa) against density (kg/m^3)

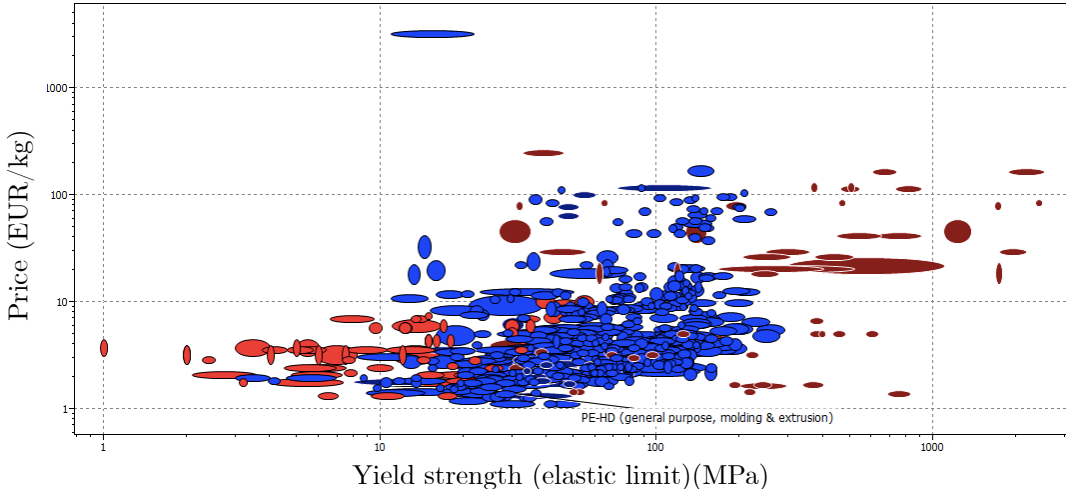


Figure 36: Yield strength (elastic limit)(MPa) against price (EUR/kg)

B Technical Drawings

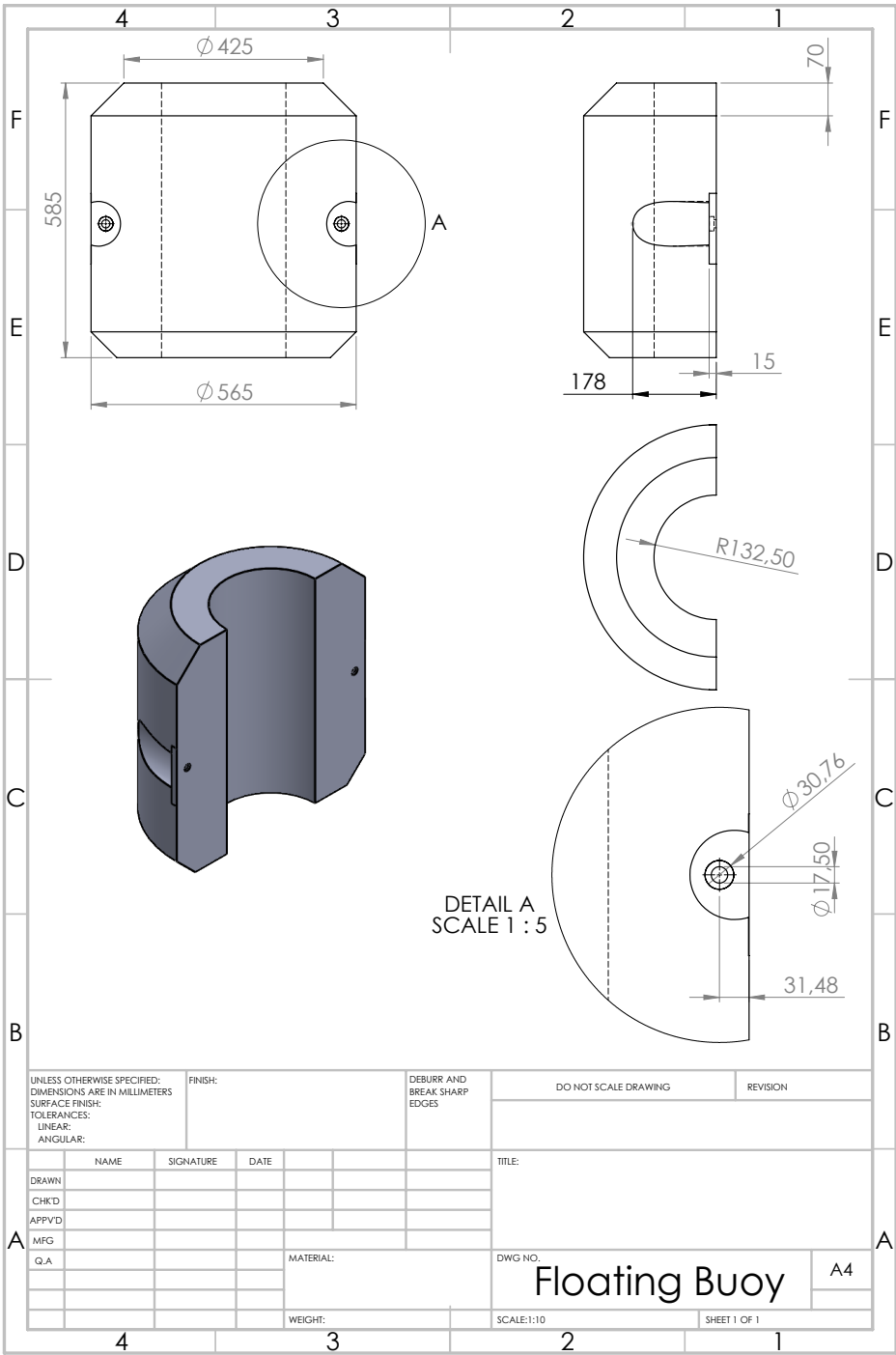
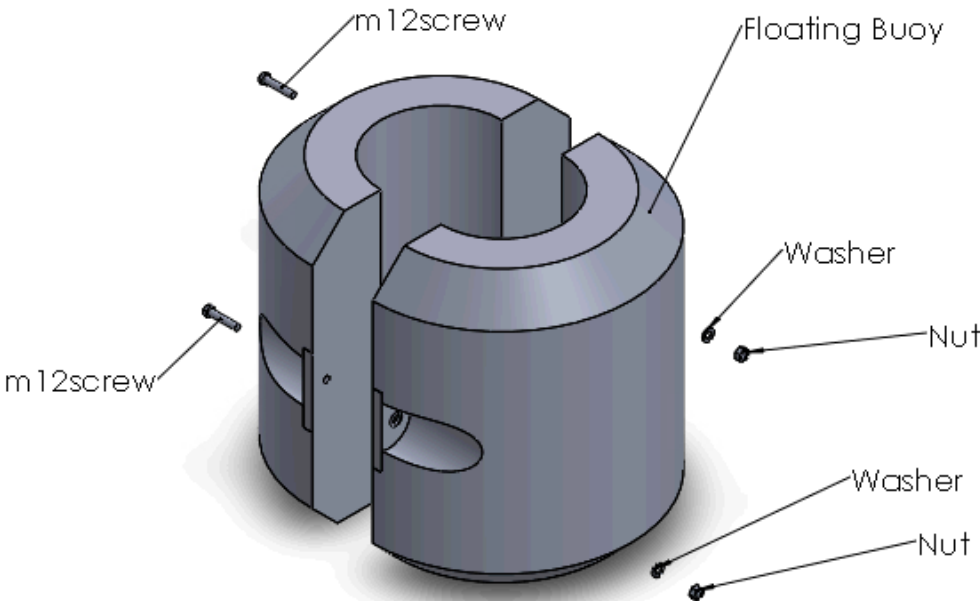


Figure 37: Technical drawing of floating buoy



ITEM NO.	PART NUMBER	DESCRIPTION	QTY.
1	Floating Buoy	Semicircular shell	2
2	m12screw	M12 Screw	2
3	Washer	M12 Washer	2
4	Nut	M12 Nut	2

Figure 38: Exploded view and BOM of the assembly of the floater

C Optimisation

```

1 clear all
2
3 % Define upper and lower bound for fmincon.m
4 lb = 0;
5 ub = 100000;
6
7 % Define variables
8 h = 3;           % Set wave height (h=3 limit for this study)
9 disp = 5;       % Set maximum surge (min at 3.0625)
10 k = 51.939;    % Umbilical stiffness
11 L = 5;         % Cable length
12 Fbnet = 398.22; % Net buoyancy force
13 Fw = 14.11;    % Mean wind force
14 Fc = 122.5;    % Mean current force
15 Fd = (1/4)*1027*h^2; % Drift force w.r.t wave height
16 Fexc = Fw + Fc + Fd; % Excitation force
17 Fmax = 25523.153; % Maximum allowable force
18
19 constants = {Fexc, k, L, Fbnet, Fmax, disp}; % Store constants
20
21 % Call Functions
22 obj_fun = @(Fpre) objective(Fpre, constants);
23 nlcon_fun = @(Fpre) nlcon(Fpre, constants);
24
25 % Initial Guess
26 Fpre0 = 2e4;
27
28 % Solver options
29 options = optimoptions('fmincon');
30 options.Algorithm = 'sqp';
31
32 % Minimization for optimal Fpre
33 Fpre_opt = fmincon(obj_fun, Fpre0, [], [], [], [], lb, ub, ...
34     nlcon_fun, options);
35
36 % Check feasibility
37 [c, ceq] = nlcon(Fpre_opt, constants);

```

Listing 3: File of inputs and minimization options (main.m)

```

1 function [f] = objective(Fpre, constants)
2
3 % Call constants
4 [Fexc, k, L, Fbnet, ~, ~] = constants{:};
5
6 syms x          % Set x as a symbol to use in solver
7 s = solve(((Fpre+k*(sqrt(x^2+L^2)- L))*x)/(sqrt(x^2+L^2))==Fexc,x,...
8             'real',true);
9 Surge = real(double(s));          % Convert x from symbol to value
10 theta = asind(Surge/sqrt(L^2+(Surge)^2)); % Calculate angular displacement
11 Fcord = Fexc/cosd(90-theta);      % Calculate Fexc perpendicular component
12
13
14 % Objective Function
15 f = Fpre + Fbnet + Fcord;
16
17 end

```

Listing 4: Objective function (objective.m)

```

1 function [c, ceq] = nlcon(Fpre, constants)
2 % Function for solving constraints
3
4 % Call constants
5 [Fexc, k, L, Fbnet, Fmax, disp] = constants{:};
6
7 % Define non equality constraint
8 ceq = 0;
9
10 % Inequality constraint calculations
11 syms x          % Set x as a symbol to use in solver
12 s = solve(((Fpre+k*(sqrt(x^2+L^2)- L))*x)/(sqrt(x^2+L^2))==Fexc,x,...
13             'real',true);
14 Surge = real(double(s));          % Convert x from symbol to value
15 theta = asind(Surge/sqrt(L^2+(Surge)^2)); % Calculate angular displacement
16 Fcord = Fexc/cosd(90-theta);      % Calculate Fexc perpendicular component
17
18 % Constraint 1
19 c(1) = Surge - disp;
20
21 % Constraint 2
22 c(2) = Fpre + Fbnet + Fcord - Fmax;
23
24 end

```

Listing 5: Constraints function for the solver (nlcon.m)

D Static Surge Displacement Analysis

```

1 clear all
2 format long
3
4 % Input
5 Fpre = 10420.820;      % Cable pretension (Fpre=12505.816 limit value)
6
7 % Variables
8 L = 5;                % Length of umbilical
9 k = 51.939;          % Umbilical stiffness
10 Fw = 14.11;          % Wind force
11 Fc = 122.5;          % Current force
12 Fmax = 25523.153;    % Maximum allowable force
13 Fbnet = 398.22;      % Net buoyancy force
14 Surge=zeros(1,25);   % Array to store surge displacement values
15 h=zeros(1,25);       % Array to store wave height values
16 theta=zeros(1,25);   % Array to store angular displacement values
17 Fcord=zeros(1,25);   % Array to store perpendicular force values
18
19 for m=1:25
20
21     h(m)=0.2+0.2*(m-1); % Wave height
22     Fd(m) = (1/4)*1027*(h(m))^2; % Drift force for varying wave height
23     Fexc = Fw + Fc + Fd(m); % Excitation force
24     syms x % Set x as a symbol to use in solver
25     x = solve(((Fpre+k*(sqrt(x^2+L^2)- L))*x)/(sqrt(x^2+L^2))==Fexc,x,...
26             'real',true);
27     Surge(m) = real(double(x)); % Convert x from symbol to value
28     theta(m) = asind(Surge(m)/sqrt(L^2+(Surge(m))^2)); % Calculate angular displacement
29
30     Fcord(m) = Fexc/(cosd(90-theta(m))); % Calculate Fexc perpendicular component
31     clear x
32     fprintf('Surge displacement for wave height of %0.1fm & pretension of %0.8eN is %0.4f m\
33             n',h(m),Fpre,Surge(m))
34     fprintf('\n')
35
36 end
37
38 if Fpre+Fbnet+Fcord(end) >=Fmax
39     fprintf('Exceeds ultimate tensile strength')
40
41 else
42     figure
43     plot(h,Surge) % Plot wave height against surge displacement
44     title(sprintf('Surge displacement of pretension %0.8eN',Fpre),...
45            'Interpreter','latex' )
46     fprintf('\n')
47     xlabel('Wave height (m)','Interpreter','latex')
48     ylabel('Surge displacement (m)','Interpreter','latex')
49     legend('Surge displacement','Location','northwest','Interpreter','latex')
50
51 end

```

Listing 6: Static surge displacement

E Static Analytical Calculations

```

1 clear all
2 format long
3
4 % Inputs
5 t_od = 0.04;           % Thickness outer layer [m]
6 t_ar = 0.03;           % Thickness armouring [m]
7 t_id = 0.03;           % Thickness inner layer [m]
8 H = 61;                % Umbilical length underwater [m]
9 h = 0.5;               % Umbilical length above sea surface [m]
10 F_exc = 273000;        % Excitation force [m/s] (NEMOH output, varies with buoy geometry)
11 v_exc = 7.5077;        % Excitation velocity [m/s] (varies with buoy geometry)
12
13 % Variables
14 rho_HDPE = 958.5;      % Density of HDPE [kg/m^3]
15 rho_GS = 7.85E3;       % Density of Galvanised Steel [kg/m^3]
16 rho_air = 1.244;       % Density of air [kg/m^3]
17 rho_sea = 1027;        % Density sea water [kg/m^3]
18 g = 9.81;             % Gravitational acceleration [m/s^2]
19 M_buoy = 2E4;          % Mass of buoy [kg]
20 C_buoy_sea = 0.6;      % Drag coefficient buoy underwater[-]
21 C_buoy_air = 0.65;     % Drag coefficient buoy above sea level[-]
22 C_umb = 18;            % Drag coefficient umbilical [-]
23 U_w = 7.8;             % Average wind velocity [m/s]
24 U_c = 0.8;             % Average ocean current velocity [m/s]
25
26 % Calculate diameters
27 hose = 0.54;           % Air hose [m]
28 is = hose+2*t_id;      % Inner sheath [m]
29 ar = is+2*t_ar;        % Armouring [m]
30 os = ar+2*t_od;        % Outer sheath [m]
31 D_umb = os;
32
33 % Calculate total volumes
34 V_PEodtot = (1/4)*pi*(os^2-ar^2)*(H+h); % Outer sheath [m^3]
35 V_PEidtot = (1/4)*pi*(is^2-hose^2)*(H+h); % Inner sheath [m^3]
36 V_ARTot = (1/4)*pi*(ar^2-is^2)*(H+h); % Armouring [m^3]
37 V_air = (1/4)*pi*hose^2*H; % Hose [m^3]
38
39 % Calculate submerged volumes
40 V_PEOdsub = (1/4)*pi*(os^2-ar^2)*H; % Outer sheath [m^3]
41 V_PEOdsub = (1/4)*pi*(is^2-hose^2)*H; % Inner sheath [m^3]
42 V_ARsub = (1/4)*pi*(ar^2-is^2)*H; % Armouring [m^3]
43
44 % Calculate total mass of components
45 M_PEtot = rho_HDPE*(V_PEodtot+V_PEidtot); % Mass PE [kg]
46 M_ARTot = rho_GS*V_ARTot; % Mass armouring [kg]
47
48 % Calculate submerged mass of components
49 M_PESub = rho_HDPE*(V_PEOdsub+V_PEOidsub); % Mass PE [kg]
50 M_ARsub = rho_GS*V_ARsub; % Mass armouring [kg]
51 M_air = rho_air*V_air; % Mass air [kg]
52

```

```

53 % Calculate total weight of components
54 W_PEtot = M_PEtot*g; % Weight PE [N]
55 W_ARTot = M_ARTot*g; % Weight armouring [N]
56 W_air = M_air*g; % Weight air [N]
57 W_buoy = M_buoy*g; % Weight of buoy [N]
58
59 % Calculate subermed weight of components
60 W_PEsab = M_PEsab*g; % Weight PE [N]
61 W_ARsab = M_ARsab*g; % Weight armouring [N]
62
63 % Buoyancy of components
64 FB_PE = rho_sea*g*(V_PEodsub+V_PEidsub); % Buoyancy PE [N]
65 FB_AR = rho_sea*g*(V_ARsab); % Buoyancy armouring [N]
66 FB_air = rho_sea*g*V_air; % Buoyancy air [N]
67
68 % Outputs
69 M_umbilical = M_PEtot+M_ARTot+M_air % Umbilical mass [kg]
70 W_umbilical = W_PEtot+W_ARTot+W_air % Umbilical weight [N]
71 FB_required = W_umbilical-(FB_PE+FB_AR+FB_air) % Required buoyancy force [N]
72 MB_required = FB_required/g % Buoy buoyancy load [kg]
73
74 % Calculate required umbilical dimensions
75 V_limit=(FB_required+W_buoy)/(9.81*rho_sea); % Limiting volume for equilibrium [m^3]
76 D_outer = sqrt((V_limit+(1/2)*pi*D_umb^2)/((1)/(2)*pi));% Limiting outer diameter buoy [m]
77 D_opt = sqrt((V_limit+(1)/(4)*pi*1.5*D_umb^2)/((1)/(4)*pi));% Optimal outer diameter buoy[m]
78 V_opt = (1)/(2)*pi*(D_opt^2-D_umb^2); % Optimal volume bouy [m]
79
80 % Wind force
81 A_wind = (1/2)*pi*(D_opt)*0.5; % Area of buoy exposed to wind [m^2]
82 F_wind = (1)/(2)*rho_air*C_buoy_air*A_wind*U_w^2;% Average wind force [N]
83
84 % Submerged surfaces
85 A_umb_underwater = (1/2)*pi*D_umb*(H-1.5); % Area of umbilical exposed to current [m^2]
86 A_buoy_underwater = (1/2)*pi*D_opt*(1.5); % Area of buoy exposed to current [m^2]
87
88 % Resultant surge force
89 F_D = (1/2)*C_buoy_sea*rho_sea*v_exc^2*A_buoy_underwater; % Drag force [N]
90 F_resultant = F_exc+F_wind-F_D % Resultant surge force [N]

```

Listing 7: Buoy dimensions script

F Wave Characteristics

```
1 function k = WaveNumbers(w,depth)
2 g = 9.81;
3 k0=w/sqrt(g*depth);
4 option=optimset('display','off');
5 k=fsolve(@(k) WaveNumFunc(k,w,depth),k0,option);
6 end
7
8 function F=WaveNumFunc(k,w,depth)
9 g=9.81;
10 F=w^2-g*k*tanh(k*depth);
11 end
```

Listing 8: Wavenumber script

```
1 function c=WaveVelocity(w,k,h)
2 c(2,:) = w./k; % Phase velocity [m/s]
3 c(1,:) = 0.5.*c(2,:).*(1.0+2.*k*h./sinh(2.0.*k*h)); % Group velocity [m/s]
4 c(3,:) = sqrt(9.81*h); % Shallow water wave phase velocity [m/s]
5 end
```

Listing 9: Wave velocities script

G Solidworks Fixtures and Meshing

The following fixtures were set up in Solidworks:

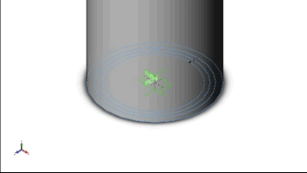
Fixture name	Fixture Image	Fixture Details
Fixed-1		Entities: 3 face(s) Type: Fixed Geometry

Figure 39: Fixtures applied on the umbilical geometry in Solidworks

Meshing a geometry of these dimensions was found to be a great complication in Solidworks. The most refined mesh possible results in meshing errors, and thus applying mesh control was essential. Figure 40 shows the mesh control applied.




Mesh Control Name	Mesh Control Image	Mesh Control Details
Control-1		Entities: 1 Solid Body (s) Units: mm Size: 198.436 Ratio: 1.5
Control-2		Entities: 1 Solid Body (s) Units: mm Size: 222.385 Ratio: 1.5
Control-3		Entities: 1 Solid Body (s) Units: mm Size: 205.278 Ratio: 1.5

Figure 40: Mesh control applied on the umbilical geometry in Solidworks

H Loads Applied in Solidworks

Figure 41 shows the loads applied to the geometry in Solidworks. Recall that the current force is extracted from Solidworks Flow Simulation, and thus Solidworks Simulation does not show it as an input load on the geometry.



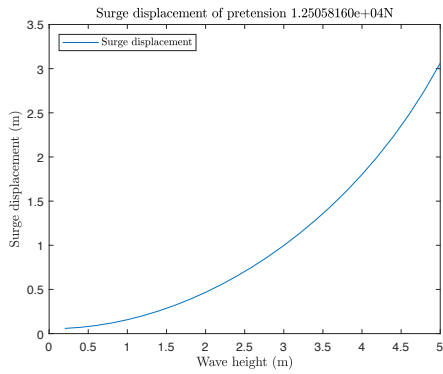
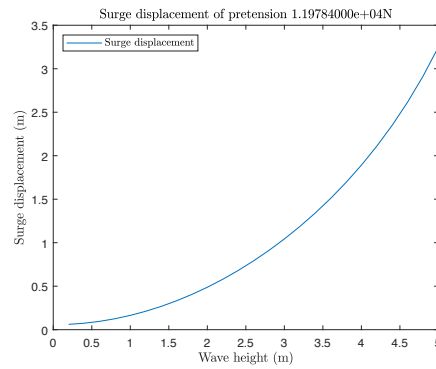
Load name	Load Image	Load Details
Force-1		Entities: 1 face(s), 1 plane(s) Reference: Front Type: Apply force Values: ---, ---, -20459.6 N
Pressure-1		Entities: 1 face(s) Type: Normal to selected face Value: 1 Units: N/m ² Equation: 1027*9.81*(("y"-2) (m) Ref Coord Sys: Coordinate System2 Coord Sys Type: Cartesian Phase Angle: 0 Units: deg

Figure 41: Loads applied on the umbilical geometry in Solidworks

I Surge Displacement Results

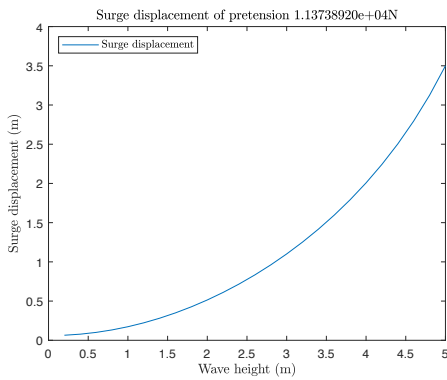


(a) Maximum displacement $\Delta x = 3.0625m$.

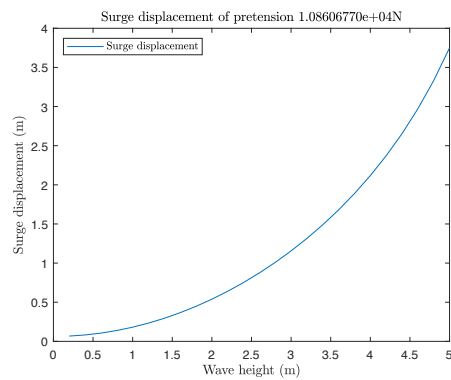


(b) Maximum displacement $\Delta x = 3.25m$.

Figure 42: Surge displacements for $F_{pre} = 12505.816N$ (a) and $F_{pre} = 11978.400N$ (b).

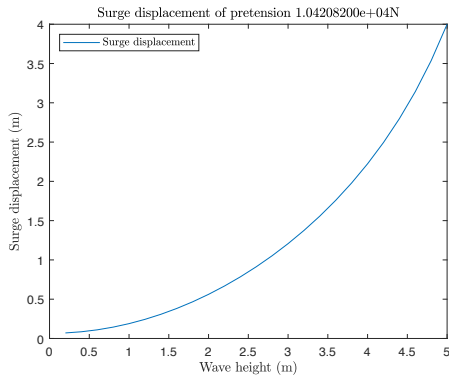


(a) Maximum displacement $\Delta x = 3.5m$.

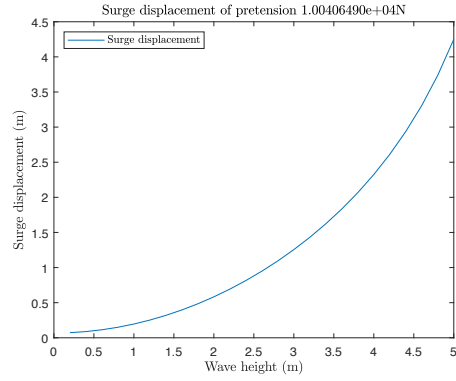


(b) Maximum displacement $\Delta x = 3.75m$.

Figure 43: Surge displacements for $F_{pre} = 11373.892N$ (a) and $F_{pre} = 10860.677N$ (b).

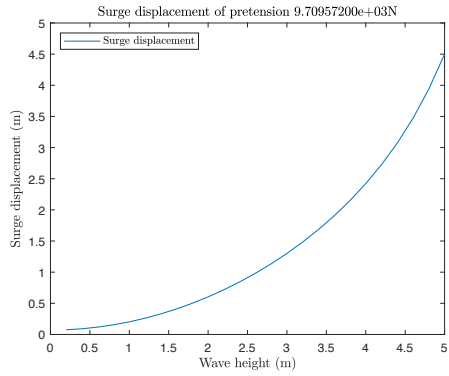


(a) Maximum displacement $\Delta x = 4m$.

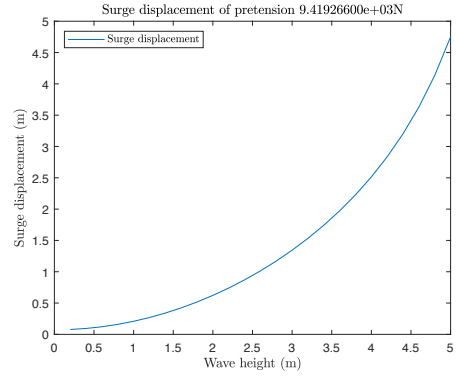


(b) Maximum displacement $\Delta x = 4.25m$.

Figure 44: Surge displacements for $F_{pre} = 10420.820N$ (a) and $F_{pre} = 10040.649N$ (b).



(a) Maximum displacement $\Delta x = 4.5m$.



(b) Maximum displacement $\Delta x = 4.75m$.

Figure 45: Surge displacements for $F_{pre} = 9709.572N$ (a) and $F_{pre} = 9419.266N$ (b).

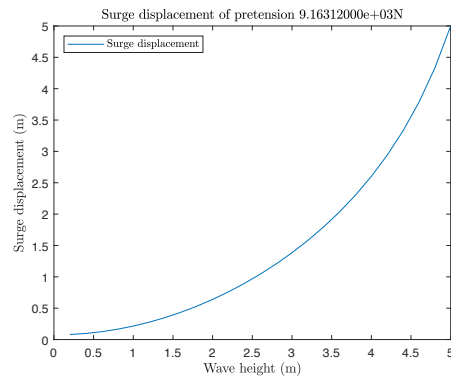
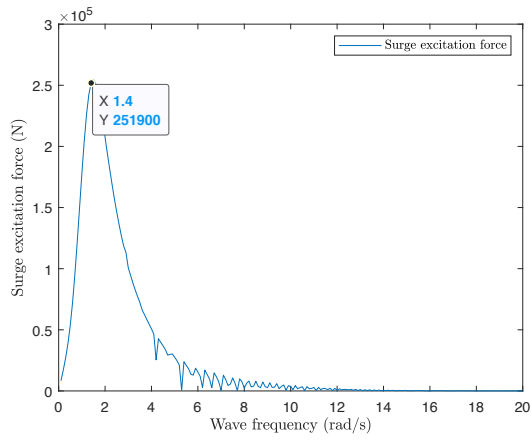
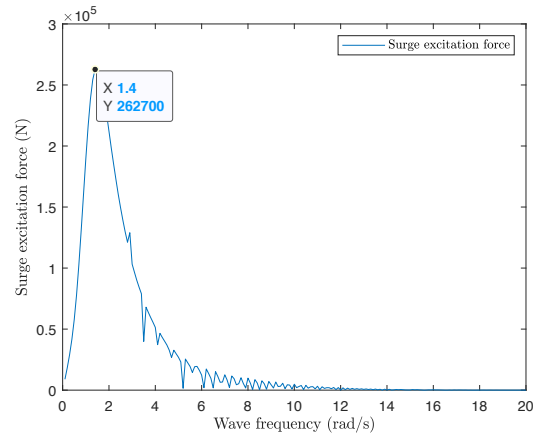


Figure 46: Surge displacement for $F_{pre} = 9163.120N$. Maximum displacement $\Delta x = 5$.

J Wave Excitation Results

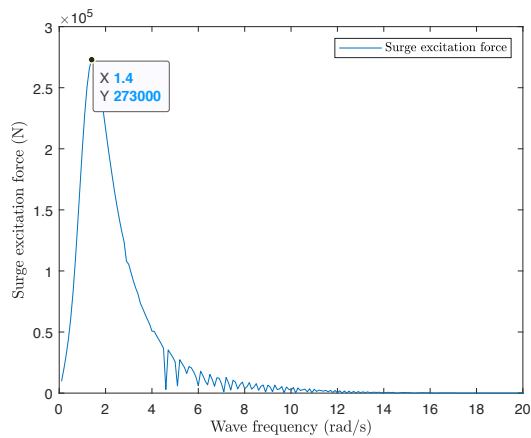


(a) Maximum excitation $F_{exc} = 251900N$ at $w = 1.4$ rad/s.

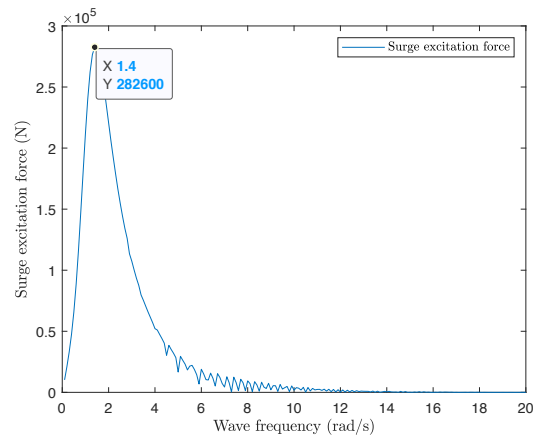


(b) Maximum excitation $F_{exc} = 262700N$ at $w = 1.4$ rad/s.

Figure 47: Surge excitation for $t = 2.5cm$ (a) and $t = 2.75cm$ (b).

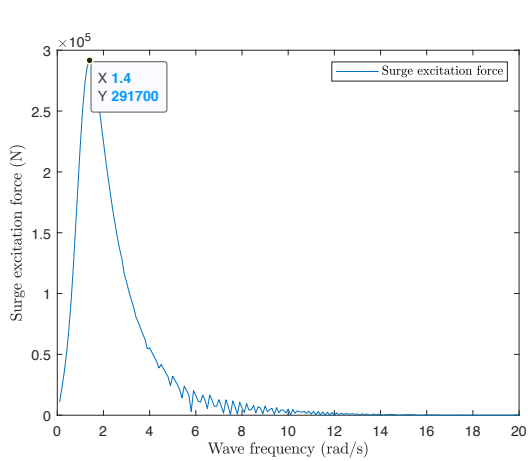


(a) Maximum excitation $F_{exc} = 273000N$ at $w = 1.4$ rad/s.

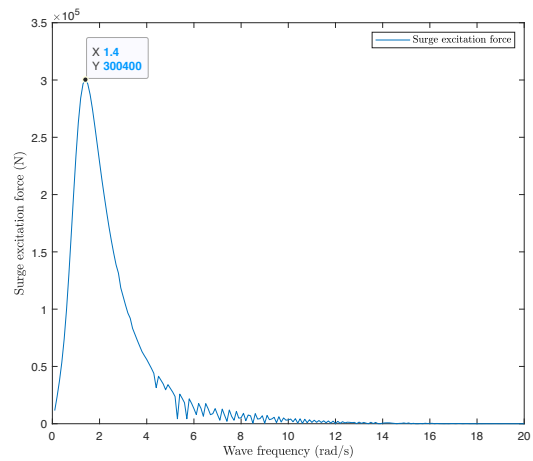


(b) Maximum excitation $F_{exc} = 282600N$ at $w = 1.4$ rad/s.

Figure 48: Surge excitation for $t = 3cm$ (a) and $t = 3.25cm$ (b).

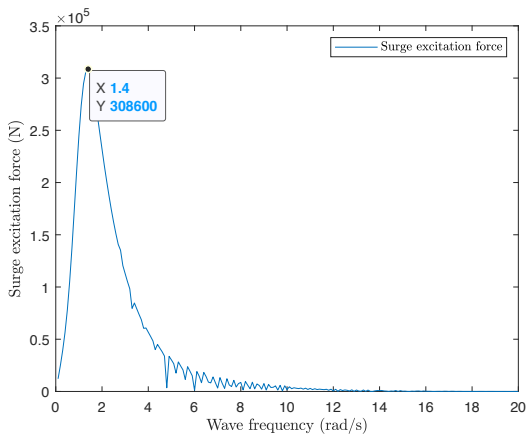


(a) Maximum excitation $F_{exc} = 291700N$ at $w = 1.4$ rad/s.

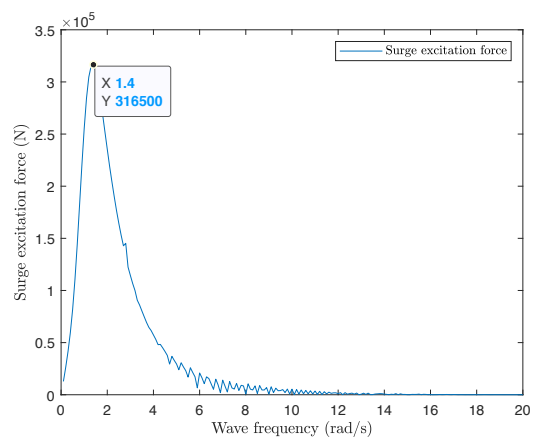


(b) Maximum excitation $F_{exc} = 300400N$ at $w = 1.4$ rad/s.

Figure 49: Surge excitation for $t = 3.5cm$ (a) and $t = 3.75cm$ (b).

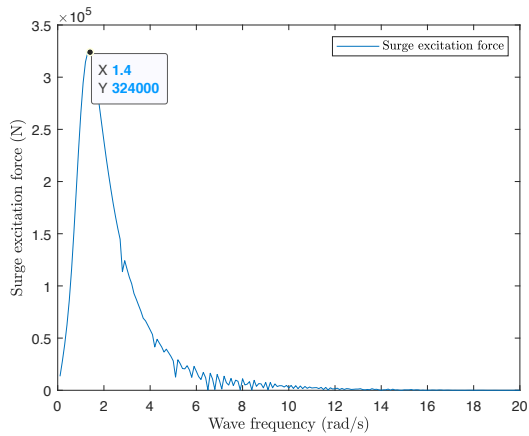


(a) Maximum excitation $F_{exc} = 308600N$ at $w = 1.4$ rad/s.

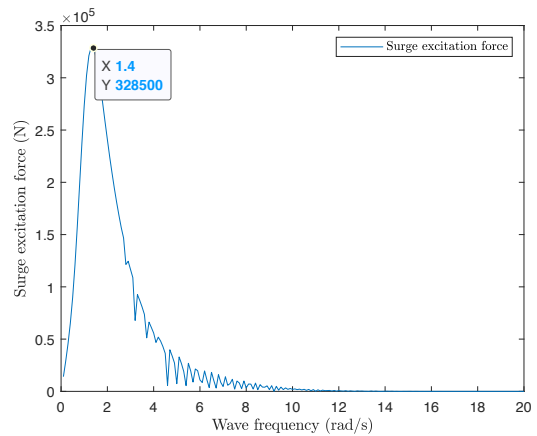


(b) Maximum excitation $F_{exc} = 316500N$ at $w = 1.4$ rad/s.

Figure 50: Surge excitation for $t = 4cm$ (a) and $t = 4.25cm$ (b).

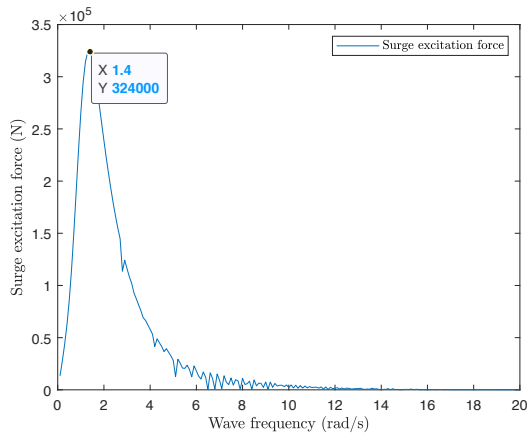


(a) Maximum excitation $F_{exc} = 324000N$ at $w = 1.4$ rad/s.

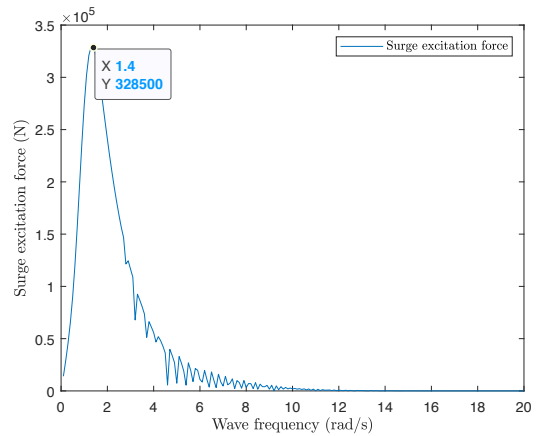


(b) Maximum excitation $F_{exc} = 328500N$ at $w = 1.4$ rad/s.

Figure 51: Surge excitation for $t = 4.5cm$ (a) and $t = 4.75cm$ (b).



(a) Maximum excitation $F_{exc} = 335300N$ at $w = 1.4$ rad/s.



(b) Maximum excitation $F_{exc} = 341900N$ at $w = 1.4$ rad/s.

Figure 52: Surge excitation for $t = 5cm$ (a) and $t = 5.25cm$ (b).

K Solidworks Simulation Results

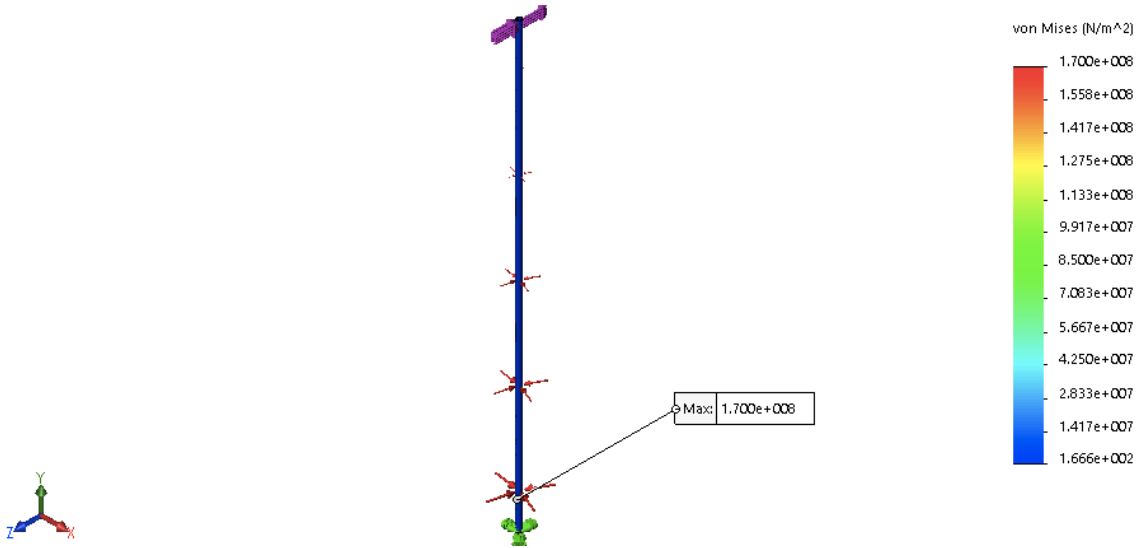


Figure 53: Von Mises stress for a 3cm armouring thickness

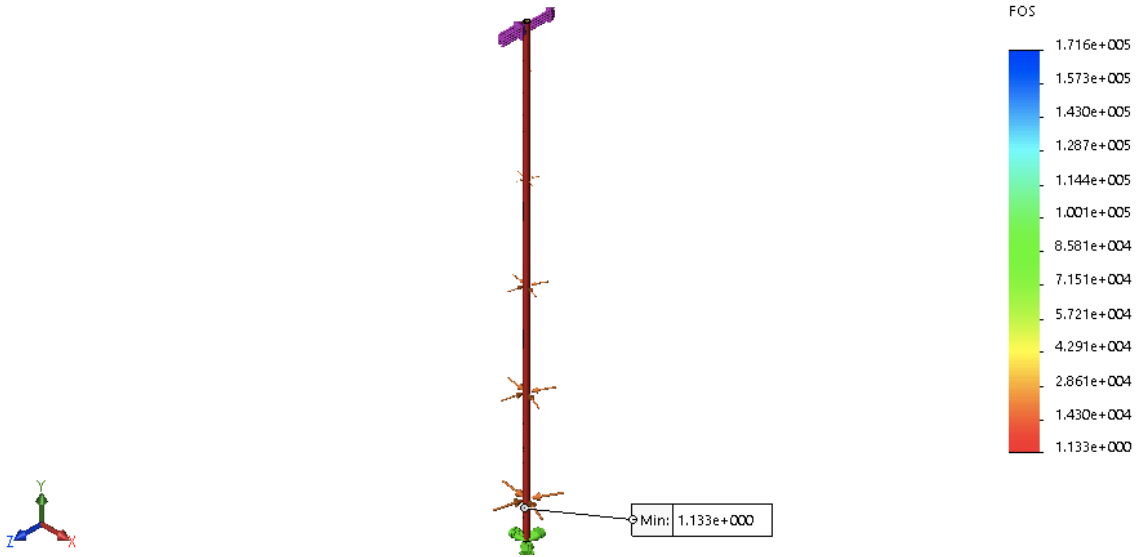


Figure 54: FOS for a 3cm armouring thickness



Figure 55: Surge displacement for a 3cm armouring thickness